PREDICTING AIR TEMPERATURES IN CITY STREETS ON THE BASIS OF MEASURED REFERENCE DATA

A thesis submitted to The University of Adelaide in fulfilment of the requirements for a degree of Doctor of Philosophy

Evyatar Erell

The School of Architecture, Landscape Architecture and Urban Design

February 2005

CHAPTER 4: EXPERIMENTAL

4.1 Overview

The nature of the project required detailed micro-meteorological data from a number of sites located sufficiently close to one another to be affected by uniform meso-scale environmental conditions, yet which are also affected by distinctly different local conditions. A monitoring experiment was designed to obtain these data, which will be described in the following sections. It was the intention to use one site in the belt of parklands surrounding the central business district as the reference location for the simulations, and a number of urban sites as the object of the calculations. A reference station was selected (Section 4.4 below) and the necessary instrumentation was installed. However, changes in the nature of the immediate surroundings of this station that occurred while the experiment was in progress introduced unexpected difficulties in describing accurately conditions at the site. It was subsequently decided to use data from the Bureau of Meteorology station at Kent Town as the reference for the simulations (Section 4.6). Data from the reference site were, however, used in the analysis of Adelaide microclimate introduced in Chapter 6.

4.2 The study area: Adelaide

The city of Adelaide (Latitude: 34.9 S, Longitude: 138.6 E) is situated at the base of the Mount Lofty Ranges, 14 kilometres inland from the centre of the eastern shore of the Gulf St. Vincent, on the south coast of the continent of Australia. It comprises the core of a metropolitan area that extends about 20 kilometres east-west and about 25 kilometres from north to south, and which has a total population of approximately 950,000 residents. It has a Mediterranean climate with hot summers (February mean temperature 23 °C), mild winters (July mean 12 °C), and an average annual rainfall of about 550 mm. The elevation of the city centre is about 50 metres above sea level.

The topography of the coastal plain is generally flat with occasional hills. However, in spite of the relatively simple topography of the majority of the populated areas of the Adelaide metropolitan area, Schwerdtfeger (1972) noted that there is a certain degree of anisotropy of meteorological characteristics: temperature differences of over 5^{o}C and major wind parameter variations among various suburban locations at similar altitudes are not uncommon. This required careful selection of the monitoring sites, especially with respect to the exposure to gully winds blowing from the slopes of the Adelaide hills.

Figure 4.1: Aerial photograph of Adelaide metropolitan area, seen from north.

Adelaide is well-suited for the experiment, for several reasons. Meteorological conditions vary from season to season and are often changeable from day to day, so data records can provide a sufficiently large range of conditions for the purpose of validation. Unlike most tropical cities, it has a substantial diurnal temperature range, and atmospheric moisture is generally low enough so that significant urban heat islands may form. Because conditions are nearly always above freezing in winter, the added complexity of dealing with freeze-thaw cycles may be avoided, and the absence of snow further simplifies the model. Because the city is generally flat, topography plays only a minor influence on meteorological conditions in the study area. The central business district of the city is sharply defined, being surrounded by a belt of parklands, and may be expected to display characteristically different environmental conditions to those occurring in the surrounding suburbs. Finally, while conditions may vary somewhat across the metropolitan area, there are no over-riding features of the climate that can be characterised as being unique to Adelaide, so that research results may be expected to have general validity and are not restricted to a unique local set of circumstances.

From a practical point of view, the cooperation of the municipal authorities, of the Adelaide City Nursery and of a number of commercial property owners facilitated the establishment of monitoring sites in the public domain. In spite of the accessibility of some of the temperature sensors, there was very little interference with the instrumentation over the entire duration of the experiment.

4.3 Criteria for selection of the monitoring sites

Criteria for selection of the test sites fall into two categories – those determining the micro-climatic properties of the site, and those affecting installation, security and maintenance of the test equipment.

Reference site

- Central Adelaide is surrounded by a belt of parklands. While the types of vegetation there differ considerably from the natural bush that covered the area prior to the construction of the city, one may assume that the microclimate there is closer to the natural state than at any other area in close proximity to the city centre. A location was therefore sought within the parklands, as close as possible to the urban sites.
- Installation of equipment: The equipment could only be left unattended for extended periods within a fenced area, inaccessible to the general public, yet allowing periodic access to the electronic loggers for data retrieval.

Urban sites

- Orientation: the street grid of central Adelaide is orthogonal, and nearly N-S/E-W in orientation. Since different orientations have varying exposure to wind and solar radiation, it was desirable to have at least one example of each orientation.
- H/W ratio: This is perhaps the most important attribute of the urban canyon. In order to have a pronounced urban effect, the desired aspect ratio is at least 1.
- Width of the street: in order to allow a sufficiently dense temperature measurement grid, the width of the street should be relatively narrow – about 5-10 metres.
- Height of buildings along canyon: The height of the buildings determines, along with the street width, the aspect ratio of the canyon. For a street 5-10 metres wide, the desired height of the buildings forming the canyon walls was therefore at least two stories. In addition, a more or less uniform height along the street, on both sides, was desirable in order to simplify characterization of the geometry.
- Length of street: The length of the street was to be sufficient to avoid edge effects at the monitoring station - at least 10 times greater than its width.
- Exposure to wind along axis of street: In the case of relatively short streets, tall massive buildings at either end of the canyon may restrict exposure to wind blowing along the axis of the street.
- Presence of A/C equipment: Heat exchangers of air conditioning plant installed adjacent to the test site would distort readings, creating conditions that are not representative of the street as a whole and which are not the result of urban geometry. It was thus essential to avoid locating sensors adjacent to such equipment.
- Presence of vegetation: The first sites to be monitored were free of the effects of sizable planted areas or trees, so as to represent an 'extreme' urban condition. The moderating effects of plants were studied in a site that was added in a later experiment.

- Vehicle traffic: While dense motor vehicle traffic is considered a source of anthropogenic heat, the present model does not account for it directly. It was considered desirable to monitor conditions in streets with light traffic only.
- Pedestrian access: Installation of sensors in locations accessible to the public was considered risky in the absence of continuous supervision. However, the lack of totally blocked-off streets in central Adelaide led to a compromise whereby sensors were installed above head height in streets with limited pedestrian traffic.
- Installation of equipment: The cooperation of the proprietors of the buildings where equipment was to be installed was essential. This involved not only mounting of sensors, but periodic access to data loggers for data retrieval. Insofar as equipment was mounted in the public realm, approval of the City Council was also required.

The equipment available permitted installation of temperature sensors at three sites – two urban ones and a third intended as the reference for the experiment. Additional data was obtained from the Bureau of Meteorology station at Kent Town, east of the city centre. Figures 4.2 and 4.3 show the locations of the stations.

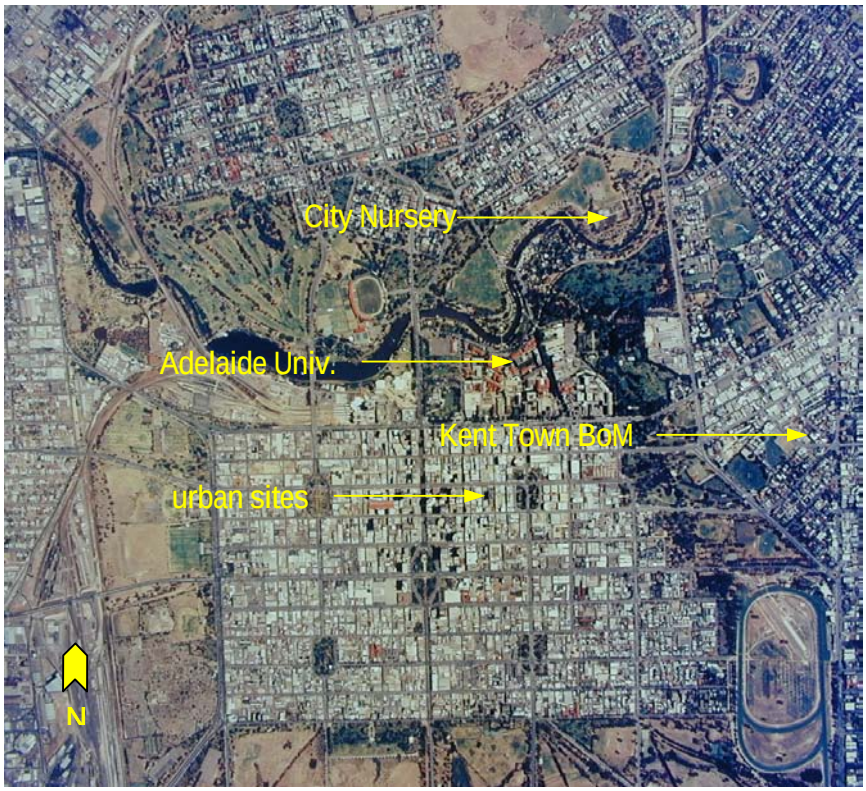

Figure 4.2: Aerial photograph of central Adelaide showing location of monitoring sites.

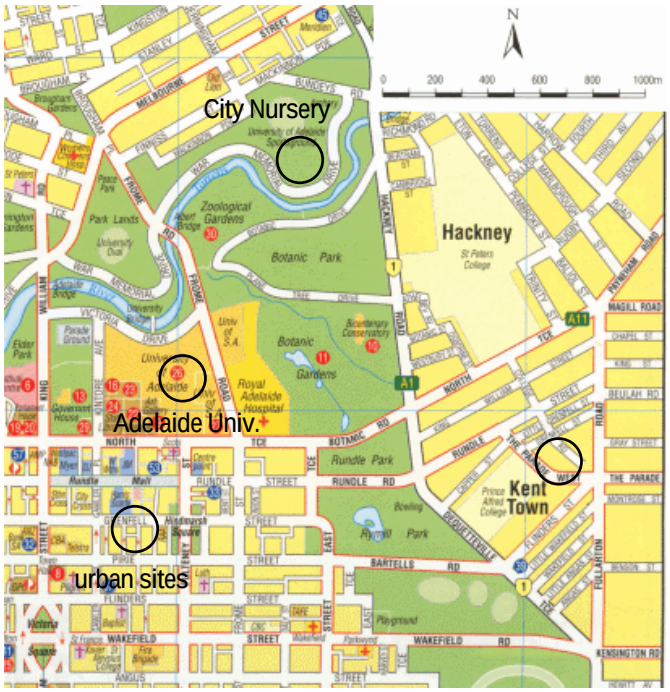

Figure 4.3: **Map of study area. Locations of monitoring stations are marked in black circles.**

4.4 The Adelaide City Nursery site

Site characteristics

The Adelaide City Nursery is located in the green belt of parklands surrounding the central business district of Adelaide, about 100 metres north of the Torrens River and approximately 2.1 kilometres northeast of the city centre. The instrumentation was installed in an open area within the premises of the Nursery, in an area characterised by mostly exposed soil, with some potted plants arranged in rows several metres away. A dense hedge about three metres tall surrounded the entire compound, which was in turn surrounded by grassland irrigated during the dry summer season.

After May 2000, the exposed soil in the area surrounding the weather station was covered with crushed asphalt gravel. In the ensuing months, more potted plants were brought close to the station, and the whole area was sprinkle-irrigated on a regular basis. By the beginning of 2001, the soil near the station had become water-logged.

Figure 4.4: View of the Adelaide City Nursery monitoring site, looking west, after the ground was covered with crushed asphalt gravel. The anemometer (not seen here) was 6m above the ground.

Instrumentation

Measurements taken at the reference station included dry bulb temperature (DBT) and relative humidity (RH) in a standard radiation screen 1.8m above the ground using a combined temperature and relative humidity sensor (UNIDATA Model 6501-E by MEA, nominal accuracy ±5%); additional dry bulb temperature in a makeshift radiation shield of the type used in the urban sites (see details in relevant sections), with a stainless steel NTC thermistor (MEA model 6507, nominal accuracy 0.2 ^{o}C); wind speed and direction 6 metres above the ground (UNIDATA Model 6504-F cup anemometer with a starting threshold of 0.8 m s^{-1} and accuracy of ±2%, magnetically coupled wind vane with 1% vectorial accuracy); soil temperature at a depth of 25cm with a stainless steel NTC thermistor (as above). Soil moisture content was determined by measuring suction using gypsum blocks at depths of 25, 50, 75 and 100cm. These had become water-logged several months after installation, and soil moisture records are considered unreliable.

4.5 The urban sites

Site characteristics

The urban sites were located in two adjacent alleys in the central business district: Chesser St., oriented approximately north-south (4.6 degrees west of north), and French St, oriented at right angles to it,

approximately east-west (See Figure 4.3). Measurements were taken about 30m north and west of the intersection between them.

Both alleys were approximately 6 metres wide, fully paved with asphalt. Adjacent buildings were of varying heights, including two office towers of approximately 50-metre height. However, the street canyon was formed primarily by lower structures – either a two-storey podium on which the office block was constructed at a setback of about 8 metres, or by two-three storey low-rise buildings (See Figures 4.4 and 4.5). The mean canyon aspect ratio near the points of measurement was approximately 1.35. The surfaces comprising the canyon walls were either of clay brick or brick veneer. Glazed openings comprised a relatively small proportion of the total surface area. French St. was totally devoid of vegetation, while a sparse deciduous vine covered a 10-metre section of Chesser St. north of the monitoring site.

Vehicular traffic in both streets was very low. French St. is used as a service road to access adjacent offices, but affords no on-street parking. The northern part of Chesser St. is blocked to prevent through-access to motor vehicles after 10 a.m. every day, except weekends, and has limited vehicular access to loading zones only. The total number of car trips on each street is estimated at no more than 20-30 per hour during office hours, and a negligible number at night and on weekends. The number of pedestrians is likewise very small – no public facilities open onto either street.

The streets were surveyed for possible local sources of heat, such as air conditioning systems (window units or compressors of central systems), and none were found. An equipment room is located on the second storey of the building at the intersection of the two streets, but no measurable heat was found to be emanating from it.

In view of the above, anthropogenic heat fluxes were considered to be very low, and due almost entirely to conduction through building envelopes.

Instrumentation

Monitoring at the urban sites consisted primarily of temperature measurement using stainless steel NTC thermistors (MEA model 6507, nominal accuracy 0.2 ^{o}C), positioned so as to allow investigation of a vertical and horizontal cross section of the street perpendicular to its axis. Each site included 5 temperature sensors: 2 each on either side of the street, 50 cm away from the building walls, 2.5 metres and 5 metres above the street; and one sensor at the middle of the street, 5 metres above road level. Relative humidity was monitored at one point only with a Rotronics thermo-hygrometer: it was assumed differences between adjacent streets would be minor, and due to variations in dry bulb temperature rather than to differences in air moisture content. Wind speed and wind direction were monitored at the intersection of the two streets, 6 metres above road level, with a VDO Instruments Model 6504-FS anemometer/wind vane (manufacturer's specifications: accuracy ±2%, threshold 0.8 m s^{-1}). The purpose of this measurement was to give indicative data only – variations of air velocity in a complex urban setting require a large number of sensors to give a detailed and accurate representation of the wind field.

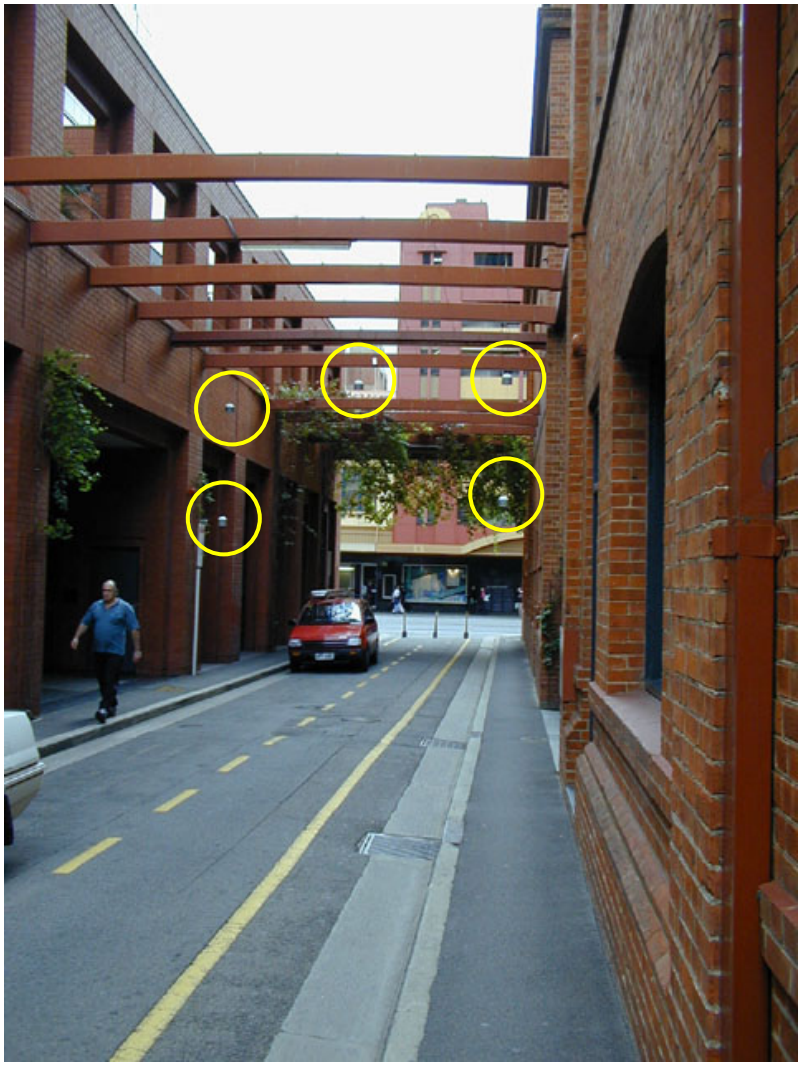

Figure 4.5: **View of the Chesser St. monitoring site, looking north. Circles show location of temperature sensors. Wind speed and direction were measured at the middle of the road, 6 metres above street level, approximately above the position where this photograph was taken.**

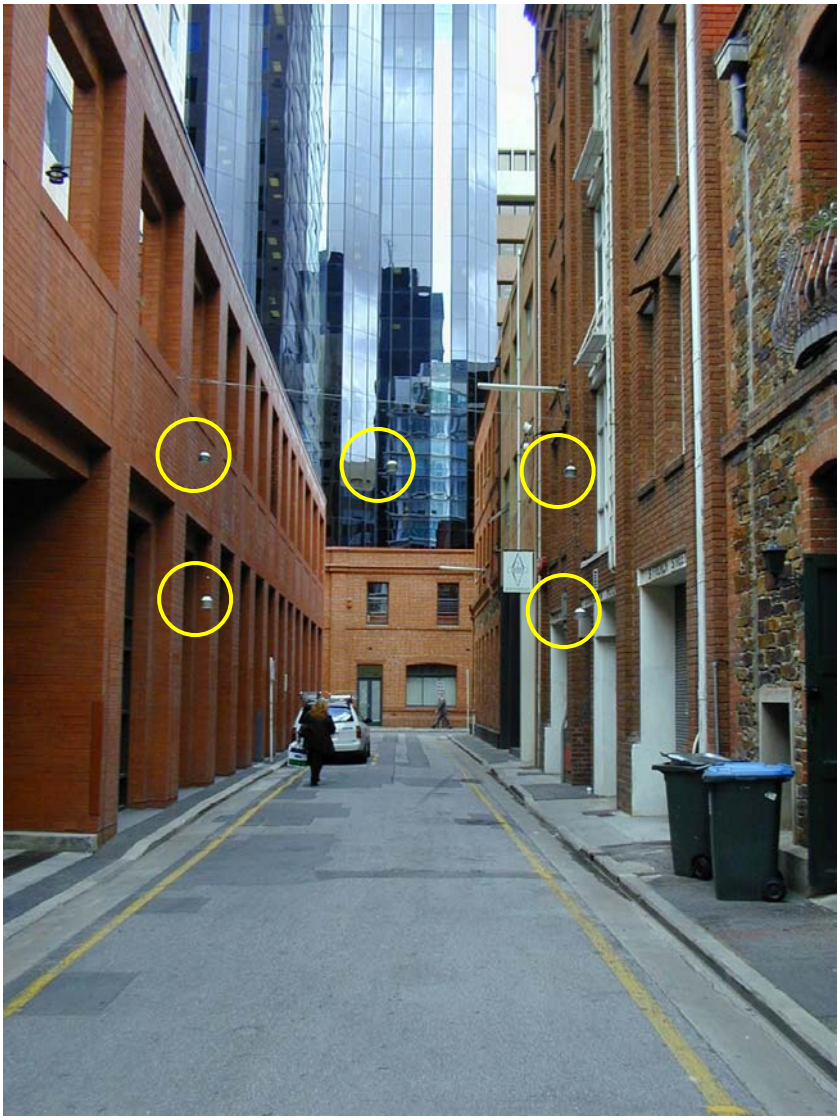

Figure 4.6: **View of the French St. monitoring site, looking west. Circles show location of temperature sensors.**

The primary interest of the current research was to predict air temperature in a variety of potential settings. This posed a practical problem, since the research program called for a relatively large number of temperature measurements to be carried out concurrently, in urban locations accessible to the general public – yet instrument screens were needed that could provide adequate protection against radiant exchange, especially solar energy. The effects of radiant exchange on thermometer readings of air temperature were recognized over 150 years ago, and eventually led to the design of the Stevenson screen in 1864. This white wooden cupboard has since become the standard instrument screen, whereby indirect ventilation is provided through the bottom, double roof and louvered sides, and thermometers placed within it give a close approximation to the true air temperature, undisturbed by the effects of direct solar or terrestrial radiation. However, the Stevenson screen was unsuitable for the urban sites: It is too bulky, too large, too obtrusive and too expensive. Furthermore, it does not give full protection from radiant exchange (World_Meteorological_Organization, 1971). Many other thermometer screens have been shown to introduce measurement error, too (Sparks, 1972; Andersson and Mathisson, 1992; van der Meulen, 1998).

A series of experiments was therefore conducted to design and evaluate a cheap, jury-rigged screen that could be installed above the street and left unattended for prolonged periods. Best results were obtained with a design resembling a standard multi-plate screen, constructed of six inverted plastic soup bowls of approximately 16cm diameter attached to each other by means of threaded rods with plastic spacers (Figure 4.7). Compared with the best available instrument screen of standard manufacture, the maximum error (in conditions of strong sunshine and no wind) was less than 0.75 ^{o}C. Subsequent tests of this type of makeshift instrument shield, along with over 10 other designs, against a mechanically aspirated standard, confirmed that it was in fact superior to other types, as well as causing smaller errors than the Stevenson screen (Erell *et al.*, 2005). However, error due to radiant load cannot be ruled out entirely when relatively large sensors are used, such as the thermistors employed in this experiment, and deviations of up to 1 ^{o}C from 'true' air temperature are nonetheless possible.

An attempt was also made to monitor the surface temperature of the road using a remote IR sensor, originally designed by the Dept. of Physics for use as a cloud detector (Clay *et al.*, 1998). The sensor comprises an infrared thermopile detector and electronic circuitry that provides a signal that is proportional to the difference in temperature between the surface seen by the detector and the temperature of the detector itself. However, evaluation of experimental data suggested that the surface temperature thus recorded was inaccurate. Experiments conducted later at the Dept. of Physics confirmed that when the temperature of the sensor is different from that of the optical components, including the sensor window and the sensor cap, the IR detector produces erroneous measurements. This condition was observed to have occurred frequently, whenever the instrument was exposed to strong sunshine. Unfortunately, there is no procedure that can be applied to the data to correct for these errors retroactively.

Figure 4.7: Jury-rigged instrument screens were used to shield thermistors from radiant exchange with the environment.

4.6 The Australian Bureau of Meteorology Station at Kent Town

Data assembled during the course of this research were also compared with meteorological data from the Bureau of Meteorology at Kent Town, which are considered representative of conditions in most of the suburbs surrounding central Adelaide. These data were analysed with two objectives in mind:

1. Having another location in which to study the effect of micro-scale, site-specific factors on air temperature.
2. Discussion of the suitability (or otherwise) of this station with respect to provision of representative data for the entire Adelaide metropolitan area. As Oke (1999) suggested, the diversity of the urban microclimate is such that a single station, however carefully selected and managed, may not be able to provide representative data for an entire city.

The Kent Town station is located in a suburban location about 2.2 kilometres east of Victoria Square, the centre of Adelaide, and about 1.7 kilometres east of the monitoring sites in Chesser St. and French St. It is also about 200 metres east of the belt of parklands surrounding central Adelaide (Fig. 4.6). Adjacent buildings are mostly one-storey residential houses, and the total distance between facades on opposite sides of the street is nearly 15 metres. The resulting sky view factor of the station is 0.93 (El Nahas, 1996).

Hourly weather records obtained from the Kent Town site include air dry bulb temperature and relative humidity (both at screen height); wind speed and direction at a standard 10m height; dewpoint temperature; atmospheric pressure; rainfall. Observations of cloud cover are reported every three hours.

Figure 4.8: Bureau of Meteorology station at Kent Town.

4.7 Solar radiation

General radiation data, assumed to be representative of all sites in the experiment, were recorded on the roof of the Architecture Building at the University of Adelaide. Global solar radiation on a horizontal surface was measured with a Middleton EP07 pyranometer, with a calibration accuracy of ±3%; diffuse radiation was measured with a similar pyranometer with a manually adjusted shadow band; net radiation was measured with a Middleton CN1 net pyrradiometer, with a calibration accuracy of ±3%. Sky temperature was measured directly using an infrared cloud detector (identical to the one used to record road surface temperature). 15-minute averages of all measurements were recorded directly on a personal computer via a 16-bit analog-digital signal converter (ADC-16 Picologger), using the software provided by the manufacturer to process the raw data.

4.8 Quality control and data collation

Weather data from all sources were read into Excel spreadsheet files each representing a continuous month-long period. Data were then de-spiked. Where short sequences of readings (up to two hours) were missing, artificial values were generated by linear interpolation with existing data.

To accommodate data from the BoM station at Kent Town and to reduce calculation time, environmental data were input to CAT at hourly intervals. Where variables were read on a shorter timescale, hourly averages were calculated.

Cloud cover, which is observed at the Kent Town weather station at intervals of three hours, was converted to an hourly format by linear interpolation. Data recorded in oktas was converted to tenths in accordance with the required format for the empirical correlations used to estimate long wave sky radiation (See Equation 3.7).

Temperature records from each of the two urban streets were investigated to assess the extent of sensor drift. Although all thermistors had been calibrated together by the supplier (MEA) in a standard bath, and their readings were mutually compared again before the system was installed in the field, minor errors appear to have developed over the duration of the experiment. This was established by comparison of the sensor readings at each of the two streets during conditions in which it was assumed readings should be identical: windy nights (wind speed at Kent Town > 10 km h^{-1}). The mean deviation of each sensor from the average for the whole group in these conditions was assumed to reflect sensor error, and a constant correction factor was therefore applied to each sensor for all records. The procedure was repeated for each monthly period, and a different correction factor was applied to each sensor accordingly. The absolute magnitude of the correction factors was never greater than 0.5 ^{o}C. Since the retroactive correction applied to the temperature readings is not based on calibration against an accurate standard, there is a risk of a bias being created between the two streets: The number of sensors is not large enough to ensure randomness in the errors. However, since the assumption that conditions in both streets were identical during the windy nights in question cannot be verified either, no attempt was made to correct for such an error, the magnitude of which may be negligible and is certainly less than about 0.3 ^{o}C.

4.9 Summary

Although the number of sites monitored was constrained by the budget available to purchase and maintain meteorological instruments, the measurements carried out nevertheless resulted in the construction of high-quality records of conditions at two urban sites. The data were organized into files of month-long periods that served as the basis for the calibration and validation of the model. In addition, the experiment provided some valuable insights into local variations in the climate of the city of Adelaide. These meteorological data are reviewed and analysed in the following chapter.

CHAPTER 5: ADELAIDE METEOROLOGICAL DATA - COMPARISON OF URBAN AND REFERENCE SITES

5.1 Overview

Weather conditions were monitored continuously for a period of approximately eleven months, from the beginning of May 2000 to the end of March 2001. Malfunctions of some of the instruments and data loggers during this extended period resulted in gaps in some of the parameters monitored. Complete (or nearly complete) data are available for the months of May, June, November, January and March, a total of 134 days. The following analysis was conducted with respect to each of these month-long periods separately and to an ensemble of the whole data.

5.2 The urban heat island

The typical urban heat island occurs in most cities when the exposed rural surroundings cool rapidly, while the city cools down more slowly because radiant loss is restricted. This mechanism usually results in maximum heat island intensity about three to five hours after sunset (Oke, 1987). The intensity then declines gradually throughout the rest of the night, as rural cooling rates decline while the city continues to lose heat at a rapid rate.

The difference in temperature observed between the urban sites in Adelaide and the reference stations at Kent Town and at the Adelaide City Nursery followed a slightly different pattern. While an urban heat island began to form following sunset, the maximum intensity typically occurred well after midnight. On many nights, high cooling rates were recorded at the reference sites until sunrise. The most intense urban heat islands - about 6-8 ^{o}C – occurred on such nights. When the maximum heat island intensity for a given night was attained before midnight, the absolute magnitude was typically much smaller – about 3-4 ^{o}C only.

The generally accepted explanation for the formation of urban heat islands suggests that intense heat islands form when radiant cooling is strong, i.e in clear sky conditions, and when wind speed is low. This pattern is evident in the Adelaide data, too, albeit with some qualifications.

Figure 5.1 shows that while maximum heat island intensity tended to occur most often when cloud cover was 0-1 tenths, substantial heat islands of over 5 ^{o}C were also observed on some occasions when cloud cover was as high as 8 or 9 tenths.

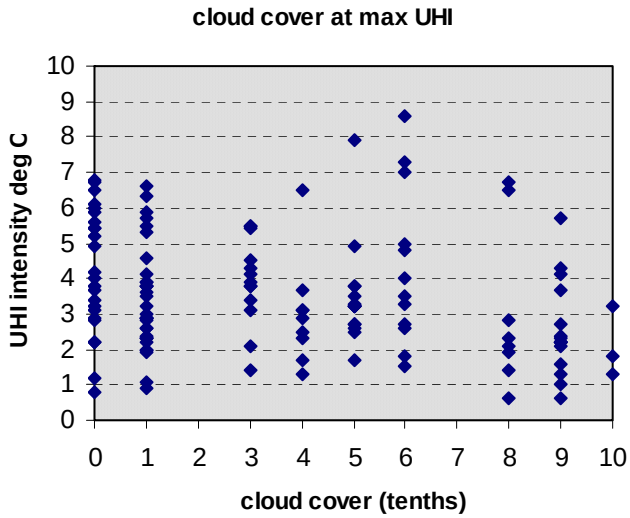

Figure 5.1: Cloud cover at the time of occurrence of the maximum heat island intensity (ensemble data for 134 days in 2000-01).

Note: Conversion of raw data from oktas to tenths and rounding to nearest whole number results in no values for 2 or 7 tenths.

Figure 5.2 shows that while intense heat islands never formed when wind speed (at 10 m height) was greater than about 3 m s^{-1}, there appeared to be no correlation between wind speed and heat island intensity at lower wind speeds. In fact, the maximum heat island during this period, 9.0°C, recorded at 4 a.m. on January 1 2001, occurred when wind speed was 1.9 m s^{-1}.

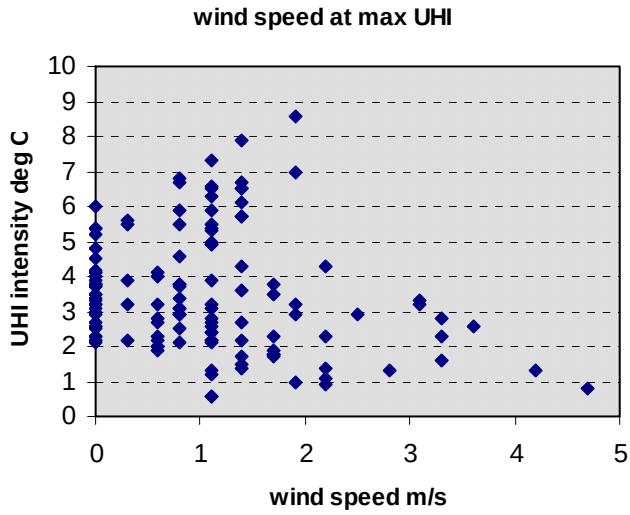

Figure 5.2: Wind speed at the time of occurrence of the maximum heat island intensity (ensemble data for 134 days in 2000-01).

Wind direction, rather than wind speed, appeared to have some effect on the intensity of Adelaide's urban heat island. Heat islands were more likely to occur when wind was blowing from the northeast, and nearly all of the most intense episodes (UHI>7.5^{o}C) were recorded when wind was blowing from this direction (Figure 5.3). The effect of wind direction was particularly dominant in the month of May, when maximum heat islands occurred almost exclusively when wind direction was between 360-060 (Figure 5.4).

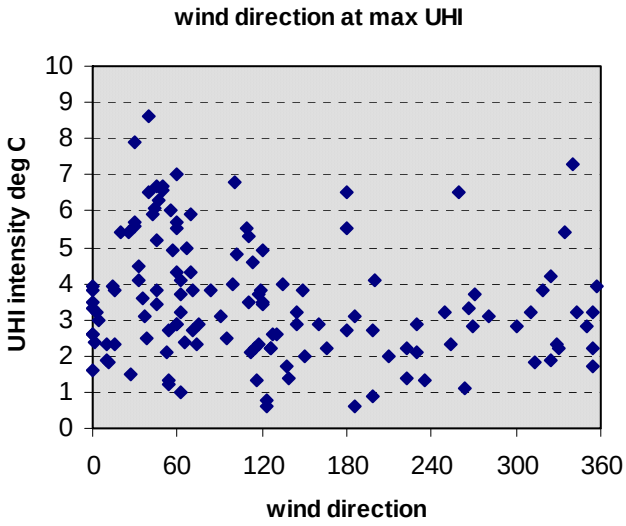

Figure 5.3: Wind direction at the time of occurrence of the maximum heat island intensity (ensemble data for 134 days in 2000-01).

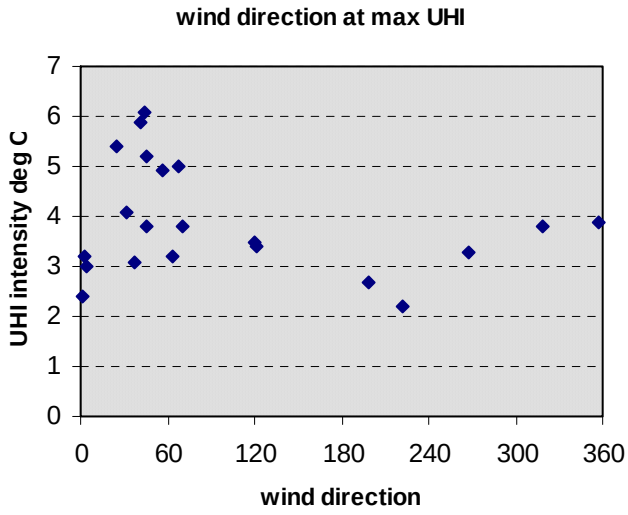

Figure 5.4: Wind direction at the time of occurrence of the maximum heat island intensity (May 2000).

Theory suggests that the nocturnal urban heat island is formed on clear nights when radiant cooling is strong, which results in low night-time temperatures in the rural station. This explanation is supported by the data for Adelaide in winter: In June, there was a definite inverse relationship between heat island intensity and the absolute temperature at the Kent Town station at the time. The data for summer is less clear-cut: In January, there appears to be no correlation between air temperature and the intensity of the heat island (Figure 5.5). A possible explanation for the lack of an apparent correlation may be that whereas the range of temperatures in June is relatively small, the variance in temperature during January is quite large, masking any underlying trends.

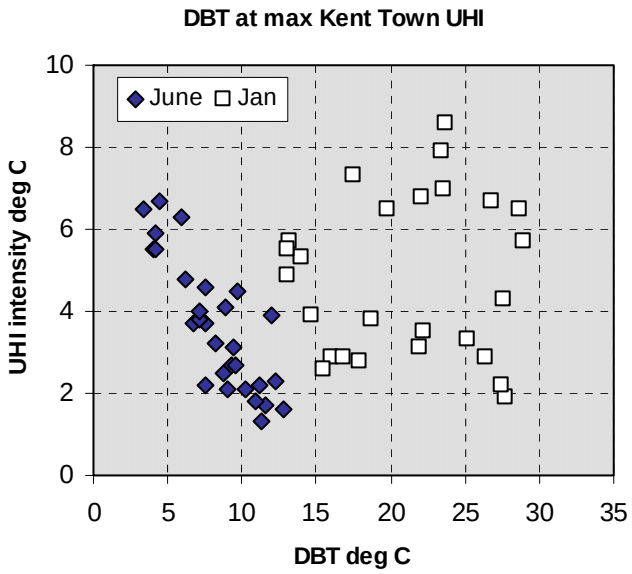

Figure 5.5: Air DBT at Kent Town at the time of occurrence of the maximum heat island intensity (June 2000, Jan 2001).

The intensity of the Adelaide urban heat island varied substantially with the seasons. It was most intense in January, when the average and maximum values were higher than in all other months, and lowest in November (Table 5.1). The table also shows a high correlation between the intensity of the heat island measured with the Kent Town station serving as the 'rural' reference and the City Nursery as the base. The City Nursery was, however, colder on many nights, and the table shows higher values for the heat island measured with respect to this station for all periods. Differences between the air temperatures at the two reference stations reflect the fact that the nursery site was more exposed, being in the belt of parklands, while the Kent Town station is on the edge of the suburban area surrounding central Adelaide, is surrounded by pavement and low-rise buildings, and has a slightly lower sky view factor.

Table 5.1: Seasonal variations in the intensity of the nocturnal urban heat island.

month	urban - Kent Town intensity of UHI [deg C]				urban - nursery intensity of UHI [deg C]			
	no. of days	min	avg	max	no. of days	min	avg	max
May 2000	21	2.2	3.9	6.1	21	1.8	5.1	8.9
June 2000	30	1.3	3.6	6.7	30	1.4	4.8	8.7
November 2000	30	0.6	2.1	4.0	0			
January 2001	26	1.9	4.8	8.6	26	1.7	4.7	8.5
March 2001	27	1.3	3.4	6.6	27	1.2	4.9	9.4
ensemble	**134**	**0.6**	**3.5**	**8.6**	**104**	**1.2**	**4.8**	**9.4**

Note: The UHI is calculated as the difference between the average of the two urban streets and the BoM weather station at Kent Town or the Adelaide City Nursery, respectively.

5.3 A daytime urban cool island

The discussion thus far has concerned the night-time phenomenon of the urban heat island. During the daytime, temperature differences between the urban sites and the reference stations were eroded, and a 'negative' heat island or urban 'cool island' became apparent. Although the intensity of this phenomenon was lower and its duration shorter than that of the nocturnal heat island, central Adelaide is nonetheless characterised by a substantial daytime urban cool island for nearly the entire year.

Examination of the meteorological data shows no apparent correlation between the intensity of the daytime urban cool island and wind speed, wind direction or cloud cover (Figures 5.6-5.8). There is, however, a definite relationship between air dry bulb temperature, atmospheric humidity and the magnitude of the UCI: Intense cool islands were recorded only when temperature was high and relative humidity was low – 10-30%, whereas cooler humid days were characterised by weak or non-existent cool islands (Figures 5.9, 5.10). This phenomenon was observed not only with respect to a timescale of days, but also on a seasonal basis. Daytime urban cool islands were least developed in June, and most intensive in January. In March, which is characterised by changeable weather, the urban cool island was weak on cool days and intense on hot ones (Table 5.2)

Note: Variations in air temperature between city-centre locations and the surrounding countryside are usually denoted by the difference '*u-r*' (urban minus rural), and urban cool islands are therefore sometimes referred to as 'negative heat islands'. The ordinate axes in Figures 5.6-5.12 have been labelled in accordance with this convention as 'UHI', negative values indicating the existence of an urban cool island.

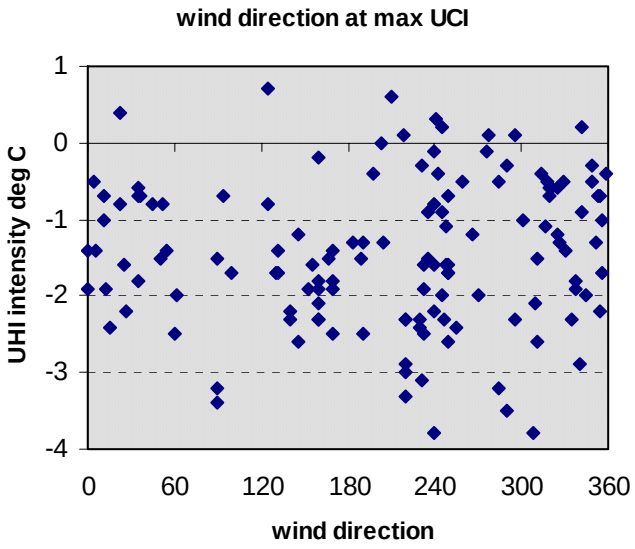

Figure 5.6: **Wind direction at Kent Town at the time of occurrence of the maximum urban cool island intensity (ensemble data for 134 days in 2000-01).**

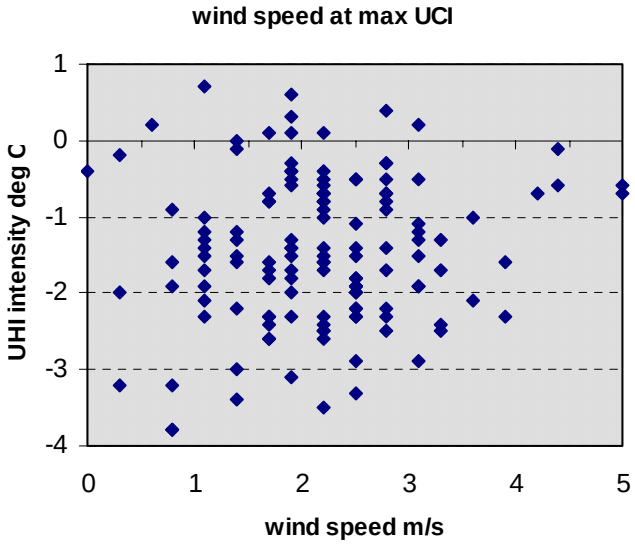

Figure 5.7: **Wind speed at Kent Town at the time of occurrence of the maximum urban cool island intensity (ensemble data for 134 days in 2000-01).**

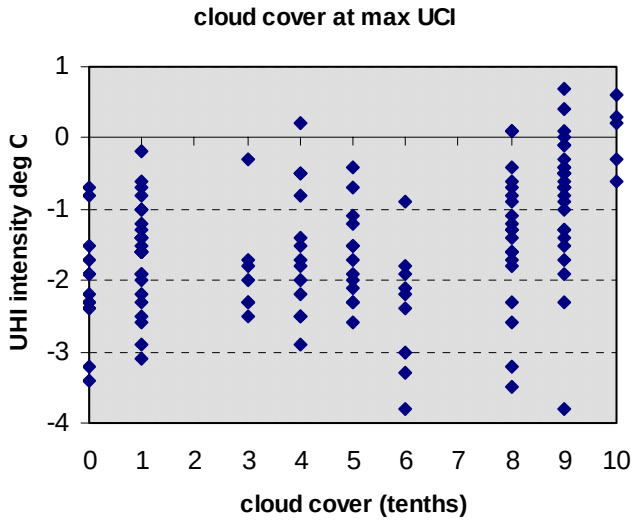

Figure 5.8: **Cloud cover at Kent Town at the time of occurrence of the maximum urban cool island intensity (ensemble data for 134 days in 2000-01).**

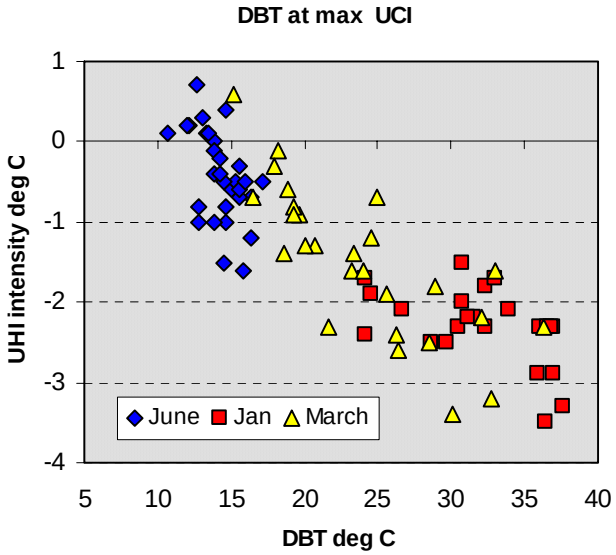

Figure 5.9: **Dry bulb temperature at Kent Town at the time of occurrence of the maximum urban cool island intensity (ensemble data for June 2000, January and March 2001).**

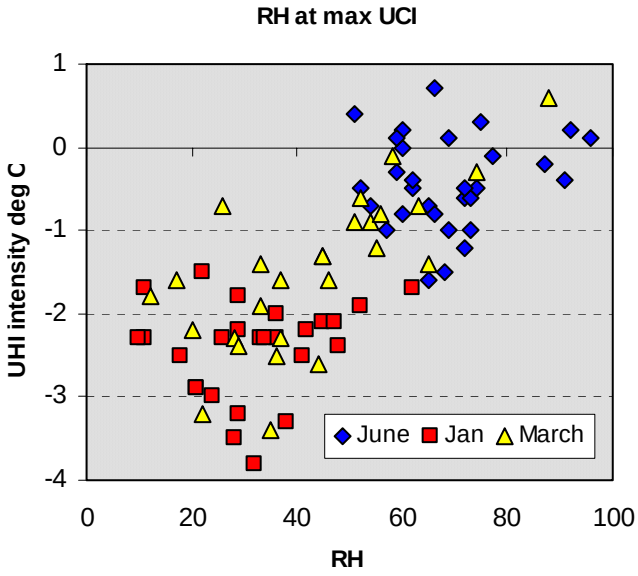

Figure 5.10: **Relative humidity at Kent Town at the time of occurrence of the maximum urban cool island intensity (ensemble data for June 2000, January and March 2001).**

Table 5.2: **Seasonal variations in the intensity of the daytime urban cool island.**

		urban - Kent Town intensity of UCI [deg C]				urban - nursery intensity of UCI [deg C]		
month	no. of days	min	avg	max	no. of days	min	avg	max
May 2000	21	-0.4	-1.1	-2.2	21	0.1	-0.9	-2.8
June 2000	30	0.7	-0.4	-1.6	30	0.7	0.1	-0.8
November 2000	30	-0.3	-1.8	-3.8	0			
January 2001	26	-1.5	-2.4	-3.8	26	-1.5	-3.4	-6.0
March 2001	27	0.6	-1.5	-3.4	27	0.5	-1.8	-3.1
ensemble	**134**	**0.7**	**-1.4**	**-3.8**	**104**	**0.7**	**-1.5**	**-6.0**

Note: The UCI is calculated as the difference between the average of the two urban streets and the BoM weather station at Kent Town or the Adelaide City Nursery, respectively. Negative values indicate that the reference sites are warmer than the urban streets.

The existence of a daytime urban cool island has been postulated by Givoni (1989), but the phenomenon has received much less attention than the nocturnal heat island. The mechanisms responsible for its evolution are less well understood, and deserve some discussion.

Net radiant exchange (Q^*) is dominated during the daytime by short-wave radiation. The widely used representation of the urban surface as a series of roughly similar building blocks interspaced with street canyons of equal depth leads to the qualitative assessment that absorption of solar energy depends, in addition to the albedo of individual surfaces, on the aspect ratio of the urban canyon: Deep narrow canyons trap more solar radiation than broader and shallower ones because multiple reflections between canyon surfaces mean that less solar radiation is reflected from the canyon floor back out of the canyon top. Many European cities fit this general scheme quite well. However, the central business districts of most U.S. and Australian cities, including Adelaide, consist of tall office blocks of varying height. This geometry results in the interception of a substantial proportion of the solar energy on extensive wall surfaces that are many tens of metres above street level. When the energy absorbed by these surfaces is given off to the adjacent layer of air in the form of sensible heat, the excess energy is advected in the roughness sublayer with limited effect on the temperature at street level. Even where tower blocks are constructed in a stepped section (where the lower two or three floors create the street façade, while the upper stories are set back by several meters), streets may receive very little direct sunlight, and may thus be substantially cooler during the daytime than more exposed areas.

Storage flux (Q_s) is related to the thermal properties of the surface and of the substrate materials. The urban heat island was attributed for many years to the supposedly higher thermal capacity of modern building materials compared with natural soil. However, a feature of the urban fabric often overlooked in this context is the increase in surface area participating in energy exchanges with the atmosphere compared to a typical rural site. Incoming solar radiation is absorbed over a much larger area, resulting in a reduced flux density per unit area of surface, lower average surface temperatures and less sensible heat emission. The effect of urban thermal mass on air temperature may be seen as being analogous to the effect of thermal mass on interior temperatures of buildings (Ratti *et al.*, 2003): One would expect the daily amplitude of urban air temperature to be reduced compared with the surrounding environment, and the minimum and maximum temperatures to be time lagged to a certain extent.

The damping effect of urban thermal mass on air temperatures is in fact clearly seen in Figure 5.11, which shows the ratio between the daily temperature amplitude at the Kent Town weather station to the amplitude at the urban streets. The correlation appears to represent a linear relationship with a ratio of about 0.7.

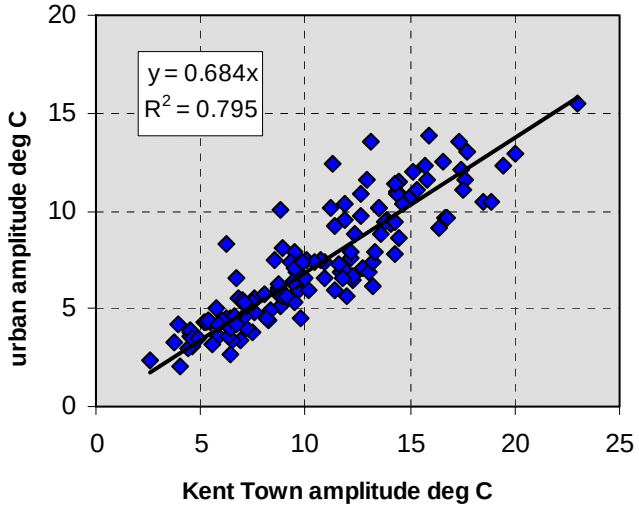

Figure 5.11: Correlation between daily amplitude of air DBT at Kent Town and at the urban street sites (June 2000, January and March 2001).

The damping effect observed above may be attributed either to the effects of urban morphology on radiant exchange or to the effects of thermal mass. The fact that the relationship is strongly linear and shows no seasonal dependence, as one would expect with solar radiation effects, favours the latter explanation. The dominant role of thermal mass is also consistent with the time lag observed between the peak of the net radiant load on the surface (about noon) and the maximum intensity of the urban cool island, which, as Figure 5.12 shows, typically occurred two to three hours later.

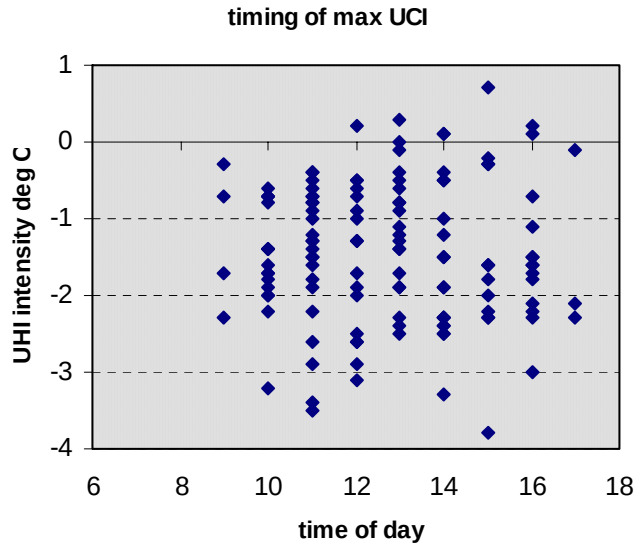

Figure 5.12: Time at which maximum intensity of the urban cool island was first observed (ensemble data for 134 days in 2000-01).

The damping effect of the city was observed both with respect to night-time differences between the city and the reference weather station, namely in the urban heat island, and in the daytime differences, here referred to as the urban cool island. In this view, the two phenomena are mirror images of each other (Figures 5.13 and 5.14).

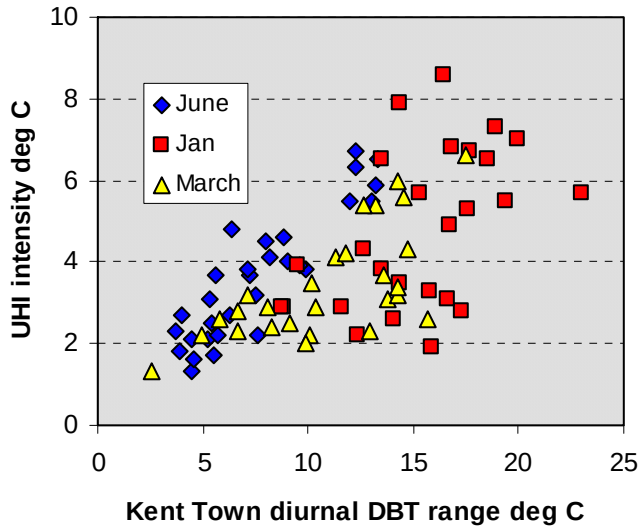

Figure 5.13: Relationship between the diurnal range of DBT at Kent Town to the maximum intensity of the urban heat island (ensemble data for June 2000, January and March 2001).

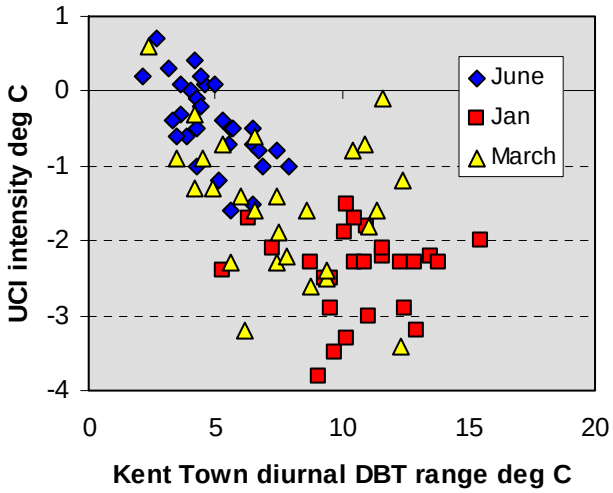

Figure 5.14: Relationship between the diurnal range of DBT at Kent Town to the maximum intensity of the urban cool island (ensemble data for June 2000, January and March 2001).

The intensity of the Adelaide daytime urban cool island is unusual when one considers the relative paucity of published data reporting similar phenomena in other cities. A partial explanation may be found in the relatively low anthropogenic heat flux (Q_f) in central Adelaide. The effect of a larger input of sensible heat would be to increase air temperature, masking the reduction in temperature due to increased thermal mass. A time-varying diurnal pattern of anthropogenic heat input, such as that reported by Sailor and Lu (2004) for a number of U.S. cities, where the magnitude of daytime flux is about two times greater than at night, is consistent with this explanation, since it would mask the daytime cool island without increasing the night-time heat island.

5.4 Street orientation

Radiant heat exchange has a central role in creating a distinct microclimate in the urban canyon. While the sky view factor and canyon aspect ratio have been singled out as the primary parameters in the evolution of the nocturnal urban heat island (Oke, 1981), less has been written about the effects of street orientation on radiant exchange during the daytime. Relatively deep canyons are exposed to direct solar radiation at different times of day, as a function of their orientation. Thus, a canyon with a north-south axis will be exposed to the sun near the middle of the day, when radiation levels are highest, while an east-west canyon may be partially or entirely shaded by adjacent buildings. In the absence of advection, one may therefore expect to find higher mid-day temperatures in the north-south canyon. In the early morning and late afternoon, the situation is reversed. However, since the intensity of solar radiation is much lower at these hours, effects on air temperature may be expected to be weaker.

Air temperature records from Chesser Street, which runs approximately north-south, and French Street, which is perpendicular to it, support the above reasoning. To simplify the comparison, the temperature difference between the streets was averaged on an hourly basis for each month. The resulting graph has a separate curve for each month, representing the typical temperature differential for each hour of the day (Figure 5.15).

While there is substantial variation among and seasons, the daily pattern is nonetheless clear: The north-south canyon was warmer during the hottest time of the day, between noon and about 3 p.m., but was generally cooler at early in the morning and before sunset. Temperature differences at night were generally smaller than 0.5 ^{o}C.

The graph shown in Figure 5.15 represents average monthly values. Actual temperature differences between the two streets were often substantially higher, reaching 3 ^{o}C or more on several occasions (Figure 5.16).

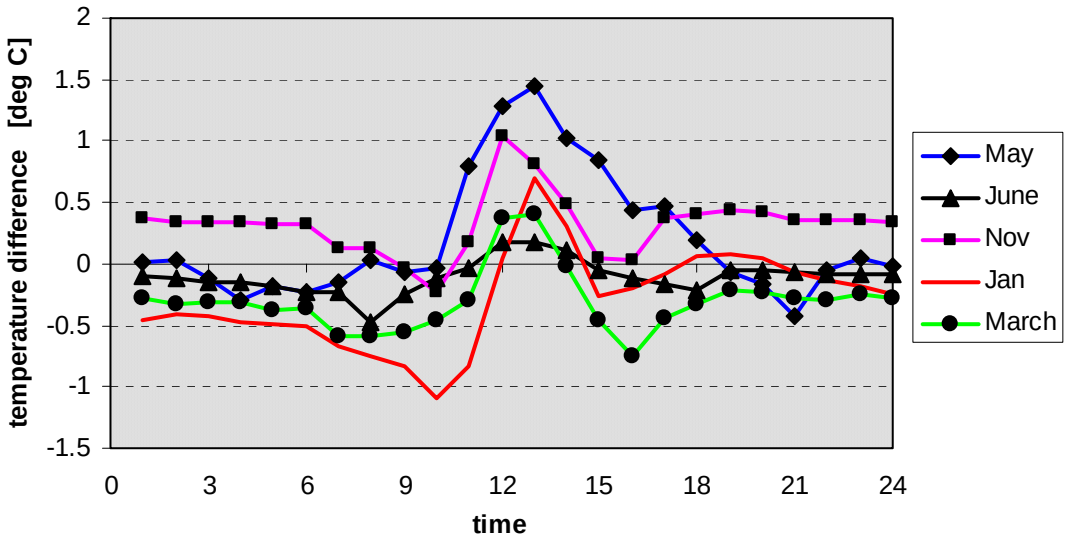

Figure 5.15: **Differences in air temperature between north-south (Chesser St.) and east-west (French St.) urban canyons. Curves represent average hourly differentials for each month. Positive values indicate Chesser St. was warmer.**

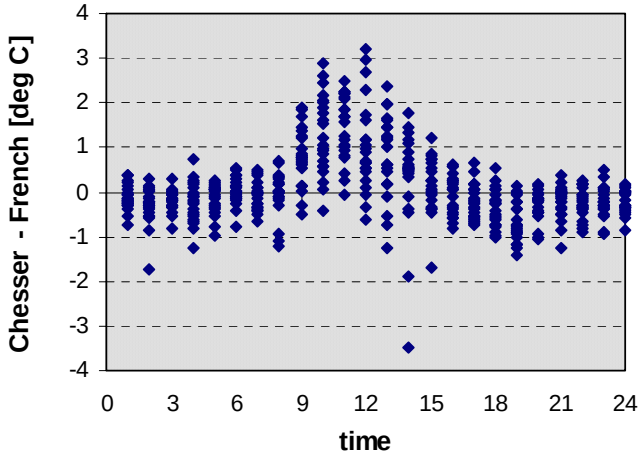

Figure 5.16: **Hourly differences in air temperature between north-south (Chesser St.) and east-west (French St.) urban canyons, during May 2000.**

5.5 Summary

Results of meteorological measurements carried out in Adelaide as part of this research show that there are significant differences between air temperature in the urban core of the city, represented by the Chesser Street site, and air temperature in less densely built suburban areas, represented by the BoM station at Kent Town, only 1650 metres away. The nocturnal urban heat island observed in most cities was noted in Adelaide, too. However, the frequent occurrence of a daytime cool island, albeit much weaker than the night-time phenomenon, is less expected. The measurements also demonstrate a measurable difference in the daily progression of air temperature between a north-south street and an adjacent east-west one.

This chapter is mainly descriptive, although the significance of the meteorological data is discussed and qualitative arguments are made in support of possible explanations for the findings. The following chapter will use these data to calibrate and validate the analytical model proposed in Chapter 3, which is designed to provide a quantitative tool for the study of urban air temperatures.

CHAPTER 6: VALIDATION OF THE CAT MODEL

6.1 Model calibration

The CAT model framework relies to a great extent on parameterisation of various components of the urban energy balance, estimating the magnitude of the fluxes on the basis of empirical correlations with meteorological quantities that are typically measured directly at standard weather stations. Some of these correlations, such as the expressions for long wave radiation received from the atmosphere, have been investigated by numerous researchers. They may be considered robust, and while not entirely free of error, their accuracy is considered sufficient (at least initially) for the purposes of this model without further calibration. A second class of parameterisations, such as those dealing with ground storage and sensible heat flux, is more recent. While the general validity of the expressions seems to be accepted by the research community, the exact values of several key constants have not yet been determined, or they may have a range of values depending on local conditions. The values incorporated in CAT for each of these empirical parameters will be discussed in the following paragraphs. Finally, a new relationship has been proposed to estimate the exchange of sensible heat that occurs at the canyon top between the canopy layer and the roughness sublayer above. The general rationale for this method was outlined in Chapter 3 above. However, the methodology used to obtain specific values for the mixing coefficient will be discussed in the last part of this section.

The monitoring program was too limited in scope to allow direct measurement of the fluxes that are parameterised within the CAT model. The methodology adopted to validate the model was therefore based on a two-stage approach: Approximate values for the various empirical parameters were introduced, based on published correlations. The model was then run on experimental data for a month-long period (June 2000), using Kent Town BoM meteorological time series as the input and mean air temperature measured in Chesser Street as the object of the simulation. The initial values of the coefficients of the empirical mixing coefficient were then modified to minimise errors in the predicted temperature in the urban canyon for this period. No further modification was attempted at this stage for the coefficients of any of the other parameterisations.

Having calibrated the model, validation was carried out by statistical analysis of the time series of predicted air temperature and measured values during several other month-long periods (May and November 2000 and March 2001). *Throughout this procedure, values of all empirical coefficients obtained earlier for the various parameterisation schemes were left unchanged*.

Calibration of the OHM model for ground storage

The OHM model, which is based on previous work by Camuffo and Bernardi (1982), is not a precise analytical formulation of energy absorption in a material: It requires empirical constants to describe the typical hysteresis between net radiant exchange at the surface, which drives the process, and energy storage. Empirical values have been obtained by researchers for a variety of surfaces, but as the table below shows, there is still a considerable range for most materials.

Table 6.1: Coefficients of the OHM model for various surface types *(Grimmond and Oke, 1999c)*.

NOTE:
This table is included on page 114 of the print copy of the thesis held in the University of Adelaide Library.

Arnfield and Grimmond (1998) suggested that the values of these coefficients may vary over time as a function of various environmental factors, such as air temperature, wind speed and exposure to solar radiation. However, the basis for their hypothesis is a numerical procedure of back-calculating values to fit measured data from one canyon (Nunez and Oke, 1977), and no general relationships are provided that may be applied elsewhere.

Since there appear to be no universally accepted values for the surface types occurring in the stations monitored in Adelaide, average values for each surface type were calculated from the table above and used in the OHM model of storage flux as a first approximation (Table 6.2):

Table 6.2: Coefficients of the OHM model for various surface types used in the CAT for Adelaide.

Location	Surface material	OHM coefficients		
		a_1	a_2 (h)	a_3 (W m^{-2})
BoM ground	Grass, planting	0.22	0.33	-20
BoM wall 1	brick	0.83	0.40	-54
BoM wall 2	brick	0.83	0.40	-54
Chesser road	asphalt	0.61	0.41	-28
Chesser wall 1	brick	0.83	0.40	-54
Chesser wall 2	brick	0.83	0.40	-54

The ground surface at the Kent Town BoM station was modelled using an average value for the two vegetated surface types in Table 6.1. In the absence of specific data either for brick or for wall surfaces in general, all walls were modelled using average values of the two listings for concrete. The values for the asphalt road in Chesser Street are the average of the three entries for asphalt above. The values of all of these coefficients were considered as being constant over time and independent of environmental conditions.

Calibration of the expression for sensible heat flux

The parameterisation for sensible heat flux proposed by De Bruin and Holtslag (1982), in the revised form given by Grimmond and Oke for urban conditions, requires two empirical constants (α and β). Values for these constants depend upon the availability of moisture at the surface, which affects the parcelling of available energy into sensible and latent heat. Previous work quoted by the same authors (Table 2.5 above) lists typical values of α and β for various landscape types. However, more recent findings suggest that these values are too high, especially for cities in dry climates or with little vegetation: The value of α was found to vary between 0.19 in Mexico City to 0.71 in Chicago, averaging about 0.45 in the cities studied, whereas the value for β in urban sites was found to be in the range –0.3 to 8.4, with an average of about 3.

Parklands surround the city centre of Adelaide, but there is very little vegetation in the immediate vicinity of the urban monitoring sites. In the absence of substantial areas of exposed pervious soil where rainfall can be collected and later evaporate over extended periods, the appropriate value of the moisture availability index in this case was therefore likely to be in the range 0.2-0.3, similar to the value reported for the downtown areas of Mexico City and Tucson (Grimmond and Oke, 2002). A constant value of 0.25 was therefore assigned to the urban sites, while the value of β was fixed at 3.

Unlike the urban site, moisture availability at the reference site at the BoM is unlikely to be constant year-round. Adelaide has a Mediterranean climate with distinct dry and wet seasons, so the use of constant annual values is probably an excessively coarse approximation. The moisture availability index α was

modified on a monthly basis, using long-term averages for precipitation and evaporation as an indication of the likely values, as follows:

Table 6.3: Values of the moisture availability parameter α for urban and reference sites in Adelaide, on a monthly basis. (Long term averages for rainfall and pan evaporation were obtained from The Australian Bureau of Meteorology, Kent Town station.)

month	J	F	M	A	M	J	J	A	S	O	N	D
α (BoM site)	0.25	0.25	0.25	0.4	0.8	1.0	1.0	0.8	0.6	0.4	0.25	0.25
α (urban site)	0.25	0.25	0.25	0.25	0.25	0.25	0.25	0.25	0.25	0.25	0.25	0.25
mean monthly rainfall (mm)	19.6	14.1	26.2	39.5	62.6	81.6	77.8	68.1	64.3	47.8	30.3	26.5
mean monthly evaporation (mm)	220.1	187.6	151.9	90.0	58.9	42.0	46.5	65.1	90.0	133.3	171.0	201.5

Note: Actual rainfall during the monitoring period was as follows: May 89.8 mm; June 81.2 mm; November 9.0 mm and March 9.4 mm.

Moisture availability is almost unrestricted during the cool, wet winter months, so α was assigned a value of 1.0, corresponding to the maximum value for parks in Table 2.5 above, or the mid-range for crops with sufficient soil moisture. During the dry summer months, α is assumed to equal about 0.25, with intermediate values assigned to the spring and autumn periods. Since the BoM meteorological station is surrounded by typical suburban low-rise buildings, β was assigned a fixed value of 10 W m^{-2}, somewhat more than the recommended value for urban sites, but less than the value of 20 W m^{-2} reported for rural locations.

The effects of short-term wetting of impervious surfaces are modelled by increasing the moisture availability index α of the urban site by (an arbitrarily fixed amount of) 0.1 during rain events, defined as rainfall in excess of 0.5mm per hour, and for a period of one hour immediately afterwards. The moisture availability index at the reference site is not adjusted, because where surfaces are pervious rainwater does not increase the amount of moisture available for evaporation unless the soil is already at field capacity – a condition reflected in the higher monthly values assigned to this site.

Values for the mixing coefficient at the top of the canopy layer

Having fixed initial (tentative) values for the coefficients incorporated in the parameterisation of the storage flux and of sensible heat production on the basis of published data, the coefficient of turbulent exchange for each of the mixing regimes described in Table 3.1 above was determined empirically using the June 2000 data, so as to minimise the error in the predicted air temperature in the urban canyon. Once appropriate values were obtained for each of the mixing regimes in both the reference site and the urban canyon (Table 6.4), they remained unchanged for the remainder of the validation procedure and were used in the simulation

of canyon air temperature in all other monitoring periods.

Table 6.4: Values of the coefficient of turbulent exchange *m* for different turbulence classes

turbulence class	mixing coefficient ***m***
highly stable	0.61
stable	0.76
neutral	0.81
turbulent	0.92

6.2 Statistical measures

As mentioned above, the on-site monitoring experiment did not include measurement of the various fluxes contributing to the total energy budget. It is therefore not possible to evaluate the accuracy of individual model components directly. The validation of the model is therefore based on comparing the final output - predicted temperatures in the urban canyon, with observed data that were assembled during the experimental phase of the project. A small separate experiment was conducted to estimate the magnitude of the error resulting from the approximation of surface temperature by the sol-air temperature (see below).

Models are often evaluated by comparison of predicted values with observed ones, yet this methodology needs to be carried out with great care. An obvious difficulty in applying standard goodness of fit tests to the predicted and observed temperature records in the current experiment is that there is a high degree of auto-correlation between the variables.

Willmott index of agreement

Willmott suggested that significance testing is inappropriate, and use of the correlation coefficient (r) or its square (r^2) insufficient (Willmott, 1981). He recommended using the observed and predicted variates' respective means ($\overline{O}$, $\overline{P}$) and standard deviations (s_o, s_p); the intercept and slope of a least squares linear regression between the variates; the errors described by the root mean squared error (RMSE), and its systematic and unsystematic components. He also proposed an index of agreement '*d*' that varies between 0 and 1, 1 indicating perfect agreement:

$$d = 1 - \frac{\sum_{i=1}^{N}(P_i - O_i)^2}{\sum_{i=1}^{N}[|P_i'| + |O_i'|]^2}$$

where $P_i' = P_i - \overline{O}$ and $O_i' = O_i - \overline{O}$. In the expression above, the denominator of the main term represents the potential error of the sample while the numerator represents the portion of this error left unexplained by the simulated variate.

Williamson degree of confirmation

Williamson identified four shortcomings of most existing techniques for validation of computer models used in thermal simulation programs (Williamson, 1995): 1) No attempt is made to take into account the severity of the validation test; 2) There is no accepted measure of the success (or otherwise) of the test; 3) Isolation of sources of error is difficult; 4) Therefore, the tests cannot be used for internal validation or algorithm tuning.

In numerous situations, the value 'v' of an input variable (or combination of several variables) can provide a fairly close approximation to the measured parameter 'm'. A model may only be considered useful if the estimated value of the parameter in question 'e' is closer to the observed value than this trivial approximation of the input variable. Williamson thus proposed a confirmation factor C_s, such that

$$C_s = U(m,v) - U(e,m)$$

where $U(m,v)$ is Theil's inequality coefficient between the measured value and the trivial variable estimate, and $U(e,m)$ is Theil's inequality coefficient between the estimated value and the measured value of the parameter in question. The maximum value of the confirmation factor is thus $U(m,v)$, when $U(e,m)$ is equal to zero, indicating perfect correlation between the measured and estimated values. The value of C_s represents a single measure combining the difficulty of the validation test and how well the model, given the input parameters, performs.

Dividing the confirmation factor C_s by $U(m,v)$ normalizes all possible values of this factor, giving a degree of confirmation D:

$$D = \frac{U(m,v) - U(e,m)}{U(m,v)}$$

The Williamson degree of confirmation has a maximum value of unity, indicating perfect agreement between predicted and measured values, and may have negative values if model predictions are poorer than the trivial approximation of the input variable.

6.3 Sensitivity analysis

The procedure employed to evaluate the sensitivity of model predictions to empirical inputs used in the parameterisation schemes was as follows:

a) The parameters used to calculate heat storage (a_1, a_2 and a_3 for each of the surfaces in the OHM model) and to model sensible heat flux (α and β) were assigned initial values for each of the sites, based on published research results (section 6.1 above).

b) The mixing coefficient (m) was assigned a value for each of the four turbulence classes described above, so as to minimise the mean error in the prediction of air temperature in the urban street canyon.

c) A single input was varied from the initial case by a predetermined amount (usually 10% and 25% above and below the base value), while all other model inputs remained constant. The effect on predicted air temperature was evaluated using three statistical measures:

- Changes in the *mean error* of the predictions are an indication of the absolute magnitude of the effect, as well as its direction, i.e. an increase in the value of the predicted air temperature relative to the observed one, or a decrease.
- Changes in the *standard deviation* of the error in prediction are an indication of the overall robustness of the model.
- Changes in the *Williamson degree of confirmation* give an indication of the effect of changes on the quality of model predictions relative to the trivial estimate (in this case, air temperature at the reference site).

Values of the Willmott index of agreement were consistently very high (above 0.95), reflecting the autocorrelation between the temperature records at the different sites, so its value as a measure of the sensitivity of the predictions was limited.

Table 6.5 (parts a-d) summarises the main findings of the analysis with respect to the parameters listed above. Cells with a shaded background display the base values for the analysis. Columns titled 'a' refer to absolute values of the standard deviation and Williamson degree of confirmation for the respective parameters. Columns titled 'r' refer to the relative (percent) change in the value of the statistic compared to the base case, normalized by the percentage change in the parameter itself.

The analysis shows that the mixing coefficients, which are applied to the total sensible heat flux in the final stage of the simulation, have the greatest effect on the accuracy of the predictions. As Figure 6.1 shows, an increase in the value of m, for any of the mixing classes, results in a proportional increase in the predicted air temperature, and hence in the difference between the predicted and observed temperatures (also referred to here as the error of the prediction). However, as Table 6.5a shows, neither the standard deviation nor the Williamson degree of confirmation respond in a similar way. These statistics, which are measures of the quality of the model, show that coefficients m_2, m_3 *and* m_4 are close to their optimal value. The value of coefficient m_1, however, is probably somewhat too high, as indicated by the fact that lower values than the base for the sensitivity analysis result in lower standard deviations of the error and a slightly higher degree of confirmation.

Coefficients α and β, which are used in the calculation of sensible heat flux (equation 3.16), likewise have a substantial effect on the outcome of the simulation. An increase in the value of both α and β at the reference site results in a decrease in the predicted temperature at the urban site, and thus as Figure 6.2 shows, a decrease in the error of prediction. A comparable increase in the value of either coefficient at the urban site has the opposite effect: The predicted temperature is higher, and the mean error of prediction greater.

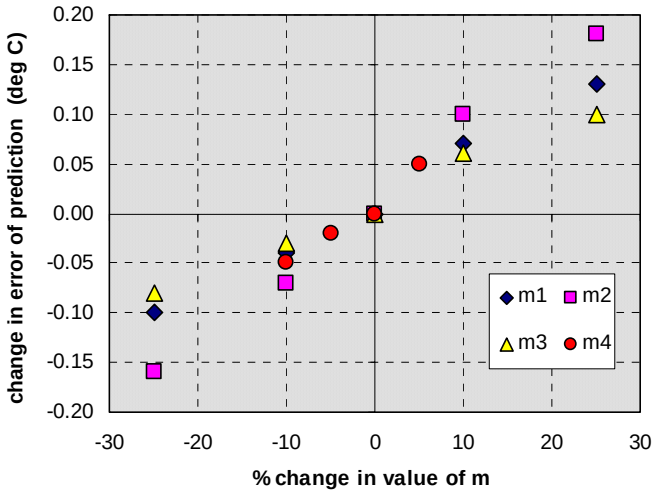

Figure 6.1: Effect of changes in the value of the mixing coefficient *m* on the error in prediction.

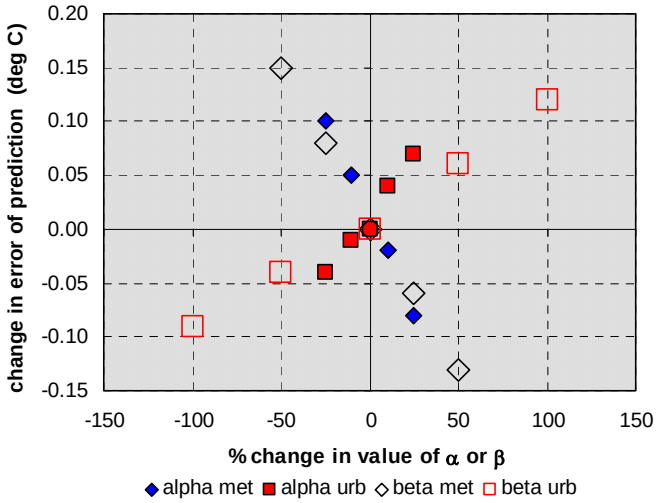

Figure 6.2: Effect of changes in the coefficients of the sensible heat equation on the error of prediction.

However, since the error is defined simply as the difference between predicted and observed temperatures at the urban site, it is the standard deviation of the error and the Williamson degree of confirmation that give an indication of the overall agreement between them. As Table 6.5b shows, both statistics indicate that the initial value of α at the urban site, 0.25, is approximately correct, while the value of α at the reference site should probably be somewhat lower than the initial value of 1.0 (for the month of June). The sensitivity analysis also suggests that the initial value of β at the reference site is probably too low, while its value at the urban site may be a little too high. The best-fit values of these coefficients for the reference and urban sites are probably about 15 and 0, respectively.

Table 6.5: Sensitivity analysis statistics.

a) Mixing coefficients

parameter	value	% change	mean error	standard deviation		Williamson degree of confirmation	
				a	r	a	r
m1	0.55	-25	-0.10	0.95	-0.12	0.581	0.068
	0.58	-10	-0.04	0.96	-0.20	0.575	0.110
	0.61	0	0.00	0.98	0.00	0.564	0.000
	0.64	10	0.07	1.02	0.40	0.547	-0.170
	0.67	25	0.13	1.06	0.32	0.527	-0.148
m2	0.68	-25	-0.16	1.04	0.24	0.539	-0.100
	0.72	-10	-0.07	1.00	0.20	0.556	-0.080
	0.76	0	0.00	0.98	0.00	0.564	0.000
	0.80	10	0.10	0.98	0.00	0.563	-0.010
	0.84	25	0.18	0.99	0.04	0.552	-0.048
m3	0.73	-25	-0.08	1.00	0.08	0.556	-0.032
	0.77	-10	-0.03	0.99	0.10	0.562	-0.020
	0.81	0	0.00	0.98	0.00	0.564	0.000
	0.85	10	0.06	0.99	0.10	0.561	-0.030
	0.89	25	0.10	1.00	0.08	0.554	-0.040
m4	0.83	-10	-0.05	1.01	0.12	0.554	-0.040
	0.87	-5	-0.02	1.00	0.20	0.560	-0.040
	0.92	0	0.00	0.98	0.00	0.564	0.000
	0.97	5	0.05	0.98	0.00	0.564	0.000

b) Sensible heat

parameter	value	% change	mean error	standard deviation		Williamson degree of confirmation	
				a	r	a	r
α met	0.900	-25	0.10	0.97	-0.04	0.567	0.012
	0.950	-10	0.05	0.98	0.00	0.566	0.020
	1.000	0	0.00	0.98	0.00	0.564	0.000
	1.050	10	-0.02	0.99	0.10	0.561	-0.030
	1.100	25	-0.08	1.00	0.08	0.555	-0.036
α urb	0.225	-25	-0.04	0.98	0.00	0.565	0.004
	0.238	-10	-0.01	0.98	0.00	0.565	0.010
	0.250	0	0.00	0.98	0.00	0.564	0.000
	0.263	10	0.04	0.99	0.10	0.563	-0.010
	0.275	25	0.07	0.99	0.04	0.560	-0.016
β met	5.00	-50	0.15	1.02	0.04	0.543	-0.02
	7.50	-25	0.08	1.00	0.08	0.555	-0.04
	10.00	0	0.00	0.98	0.00	0.564	0.000
	12.50	25	-0.06	0.97	-0.04	0.570	0.02
	15.00	50	-0.13	0.96	-0.04	0.573	0.02
β urb	0.0	-100	-0.09	0.97	-0.01	0.569	0.01
	1.5	-50	-0.04	0.98	0.00	0.567	0.01
	3.0	0	0.00	0.98	0.00	0.564	0.000
	4.5	50	0.06	0.99	-0.97	0.559	-0.01
	6.0	100	0.12	1.00	0.02	0.553	-0.01

c) Heat storage – reference site

parameter		value	% change	mean error	standard deviation		Williamson degree of confirmation	
					a	r	a	r
ground	a1 met	0.165	-25	0.00	0.98	0.00	0.568	0.016
		0.198	-10	0.00	0.98	0.00	0.566	0.020
		0.220	0	0.00	0.98	0.00	0.564	0.000
		0.242	10	0.01	0.99	0.10	0.563	-0.010
		0.275	25	0.01	0.99	0.04	0.561	-0.012
	a2 met	0.248	-25	0.00	0.99	0.04	0.562	-0.008
		0.297	-10	0.00	0.99	0.10	0.563	-0.010
		0.330	0	0.00	0.98	0.00	0.564	0.000
		0.363	10	0.00	0.98	0.00	0.565	0.010
		0.413	25	0.00	0.98	0.00	0.566	0.008
	a3 met	-15.000	-25	-0.04	0.97	-0.04	0.570	0.024
		-18.000	-10	-0.01	0.98	0.00	0.566	0.020
		-20.000	0	0.00	0.98	0.00	0.564	0.000
		-22.000	10	0.02	0.99	0.10	0.561	-0.030
		-25.000	25	0.05	1.00	0.08	0.557	-0.028
walls	a1 met	0.623	-25	0.00	0.98	0.00	0.567	0.012
		0.747	-10	0.00	0.98	0.00	0.565	0.010
		0.830	0	0.00	0.98	0.00	0.564	0.000
		0.913	10	0.01	0.99	0.10	0.563	-0.010
		1.038	25	0.01	0.99	0.04	0.561	-0.012
	a2 met	0.300	-25	0.00	0.99	0.04	0.564	0.000
		0.360	-10	0.00	0.99	0.10	0.564	0.000
		0.400	0	0.00	0.98	0.00	0.564	0.000
		0.440	10	0.00	0.98	0.00	0.564	0.000
		0.500	25	0.00	0.98	0.00	0.564	0.000
	a3 met	-40.500	-25	-0.04	0.97	-0.04	0.570	0.024
		-48.600	-10	-0.01	0.98	0.00	0.566	0.020
		-54.000	0	0.00	0.98	0.00	0.564	0.000
		-59.400	10	0.02	0.99	0.10	0.561	-0.030
		-67.500	25	0.05	1.00	0.08	0.556	-0.032

d) Heat storage – urban site

parameter		value	% change	mean error	standard deviation		Williamson degree of confirmation	
					a	r	a	r
ground	a1 urb	0.458	-25	0.01	0.99	0.04	0.562	-0.008
		0.549	-10	0.00	0.99	0.10	0.563	-0.010
		0.610	0	0.00	0.98	0.00	0.564	0.000
		0.671	10	0.00	0.98	0.00	0.565	0.010
		0.763	25	0.00	0.98	0.00	0.566	0.008
	a2 urb	0.308	-25	0.00	0.98	0.00	0.564	0.000
		0.369	-10	0.00	0.98	0.00	0.564	0.000
		0.410	0	0.00	0.98	0.00	0.564	0.000
		0.451	10	0.00	0.99	0.10	0.564	0.000
		0.513	25	0.00	0.99	0.04	0.564	0.000
	a3 urb	-21.000	-25	0.06	0.99	0.04	0.558	-0.024
		-25.200	-10	0.03	0.99	0.10	0.562	-0.020
		-28.000	0	0.00	0.98	0.00	0.564	0.000
		-30.800	10	-0.02	0.98	0.00	0.566	0.020
		-35.000	25	-0.05	0.98	0.00	0.568	0.016
walls	a1 urb	0.623	-25	0.00	0.99	0.04	0.563	-0.004
		0.747	-10	0.00	0.99	0.10	0.563	-0.010
		0.830	0	0.00	0.98	0.00	0.564	0.000
		0.913	10	0.01	0.98	0.00	0.564	0.000
		1.038	25	0.01	0.98	0.00	0.565	0.004
	a2 urb	0.300	-25	0.00	0.98	0.00	0.564	0.000
		0.360	-10	0.00	0.98	0.00	0.564	0.000
		0.400	0	0.00	0.98	0.00	0.564	0.000
		0.440	10	0.00	0.99	0.10	0.564	0.000
		0.500	25	0.00	0.99	0.04	0.564	0.000
	a3 urb	-40.500	-25	0.29	1.03	0.20	0.520	-0.176
		-48.600	-10	0.11	1.00	0.20	0.552	-0.120
		-54.000	0	0.00	0.98	0.00	0.564	0.000
		-59.400	10	-0.11	0.97	-0.10	0.570	0.060
		-67.500	25	-0.30	0.95	-0.12	0.563	-0.004

Compared with the values of the coefficients of the sensible heat parameterisation, the values of the coefficients of the OHM model of heat storage have only a minor effect on the result of the prediction of air temperature. There are several reasons for this. First, the storage flux is smaller in magnitude than other components of the heat balance for much of the time, so any error in its calculation has a smaller effect on the final outcome of the simulation. Second, if the area of a particular surface is small in comparison to the total area of the site, as is the case with canyon walls at the reference site, the effect of heat storage at this surface becomes proportionally smaller. Finally, if the two sites incorporate similar materials, for example wall surfaces, it is only the difference in surface area between them that causes a temperature deviation, and the effect of an error in describing heat storage is thus reduced. It is not surprising, therefore, that in a relatively deep street canyon, such as the urban site in Adelaide, heat storage occurs mostly in the walls. As Table 6.5d shows, this difference is due mostly to coefficient a_3.

6.4 The sol-air temperature as an approximation of real surface temperature

CAT uses the sol-air temperature of a surface as an approximation of its true temperature when calculating the long wave radiation emitted from it, as part of the model for net radiant exchange. The correlation between the two measures and the magnitude of the error resulting from this approach were assessed in a separate, short-term monitoring experiment conducted at Sde Boqer, Israel. The surface temperature of a dry loess soil was measured for several days using copper-constantan thermocouples with a very fine junction (diameter approximately 0.3 mm) embedded just below the surface. Measurement of air temperature, wind speed and global solar radiation were carried out in an adjacent meteorological station about 100 metres away. The (measured) albedo of the soil was 0.35, and long wave emissivity is estimated to be approximately 0.9. Weather conditions throughout the experiment, carried out in July 2001, were clear and sunny with light winds.

Figure 6.3 summarises the results of the experiment. At night, surface temperature appears to track air temperature at screen height, but the difference – as much as 3.0 ^{o}C just before sunrise, may not always be negligible. During the daytime, intense radiant loads result in an elevation of surface temperature by as much as 22 ^{o}C. In comparison with air temperature, the sol-air temperature is a much better approximation of surface temperature (Figure 6.4).

The good fit between surface temperature and sol-air temperature observed at the Sde Boqer site is reassuring, but the validity of the result is probably restricted to dry, relatively massive surfaces. Since the calculation of the sol-air temperature does not comprise an energy balance, it does not take into account a number of factors, such as the effects of evaporation on surface temperature. The approximation of the surface temperature of moist soils or of vegetated surfaces by this method is thus likely to be less accurate.

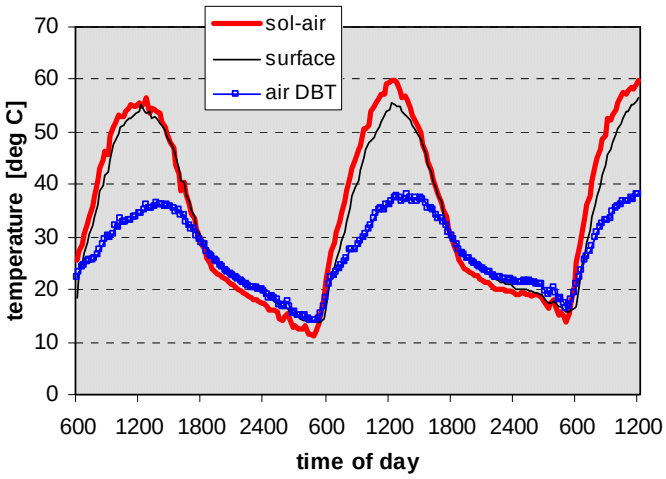

Figure 6.3: **Air, surface and calculated sol-air temperature for a dry loess soil at Sde Boqer, July 8-10 2001.**

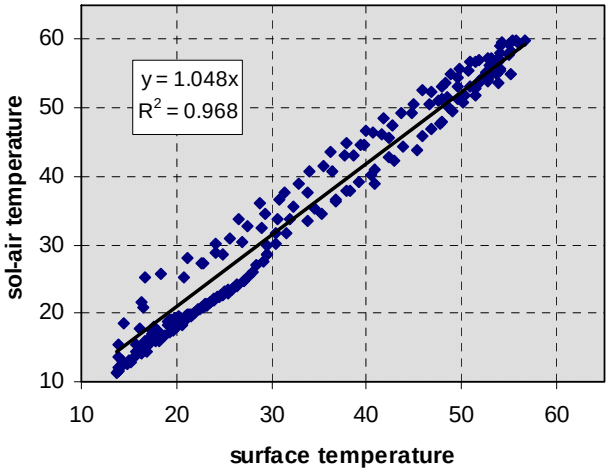

Figure 6.4: **Correlation between measured surface temperature and calculated sol-air temperature.**

6.5 Simulation results

As already indicated, the primary method for validating the CAT computer model is by comparison of predicted air temperature in the urban canyon with observed temperature measured over extended periods in the monitoring campaign. The code was calibrated by introducing appropriate values to the parameterisation schemes for storage flux and sensible heat using the measured air temperature in the urban canyon during the month of June to 'teach' the model (Section 6.2 above).

Graphic output

A first indication of the goodness of fit of the predictions may be gained by visual inspection of a graphic output of the results. Having used the June data to calibrate the model, observations from other periods were used to evaluate its performance. Figure 6.5 shows the observed and predicted air temperature at the Chesser Street site for two ten-day periods during the month of May 2000, as well as temperature at the BoM site used as the reference for the simulation. The graphic description of daily weather is intended only as a general indication of conditions, and is based mainly on cloud cover, classified as follows: *sunny* – average cloud cover for the 24-hour period 0-2 tenths; *mainly sunny* – 2-4 tenths; *partly cloudy* – 4-7 tenths; *overcast* – 7-10 tenths. Days in which total rainfall exceeded 1 mm are depicted as *rainy*.

The periods in question were selected because they are characterised by a variety of weather conditions, alternating between dry mostly sunny days and overcast rainy ones. During these sequences, the temperature difference between the BoM station and the Chesser Street site varied from being negligible to about 5 degrees, providing a rigorous test of the suitability of CAT to predict air temperature in changing environmental conditions. The graphs indicate that the program is capable of reproducing the main features of temperature evolution in the street canyon: The nocturnal heat island that occurred on several days was simulated correctly, albeit with a slight tendency to under-predict its intensity, as were temperatures on cloudy or rainy days.

The difference between observed and predicted values was then plotted against several environmental indicators measured at the reference site and against time of day, to test for any systematic error in the simulation. Figure 6.6 (a) shows that the relationship between the error and air dry bulb temperature appears to be random, implying that there is no bias for either warm or cool weather conditions. Cloud cover (Figure 6.6(b) may be interpreted in this context as an overall descriptor of weather conditions: The lack of correlation between error and cloud cover demonstrates that the CAT code is not limited to fair weather, for instance. Figure 6.6 (c) is a test of the assumption that advection may be ignored in the simulation. Since land cover in the vicinity of the test sites is not uniform, advection from particular source areas would have appeared as a bias on the graph. The random distribution of the error with respect to wind direction therefore indicates that for the site in question, at least, advected heat is not a major source of error in the simulation. Figures 6.6(d) and (e) may be interpreted as a proxy for atmospheric stability, in addition to displaying the relationship between the error and wind speed and global solar radiation, respectively. The only variable that displays what appears to be a non-random relationship with the error in prediction is time of day, shown in Figure 6.6 (f). The relationship is relatively weak, and the lack or correlation with any of the environmental variables does not suggest a specific mechanism to explain this anomaly. It is worth noting in this context that the correlation between time of day and the error in prediction for the months of June and November 2000 and for March 2001 do not display the same pattern.

Finally, Figures 6.7 and 6.8 show temperature predictions for November 2000 and March 2001, which will be discussed in conjunction with the statistical analysis in the following section.

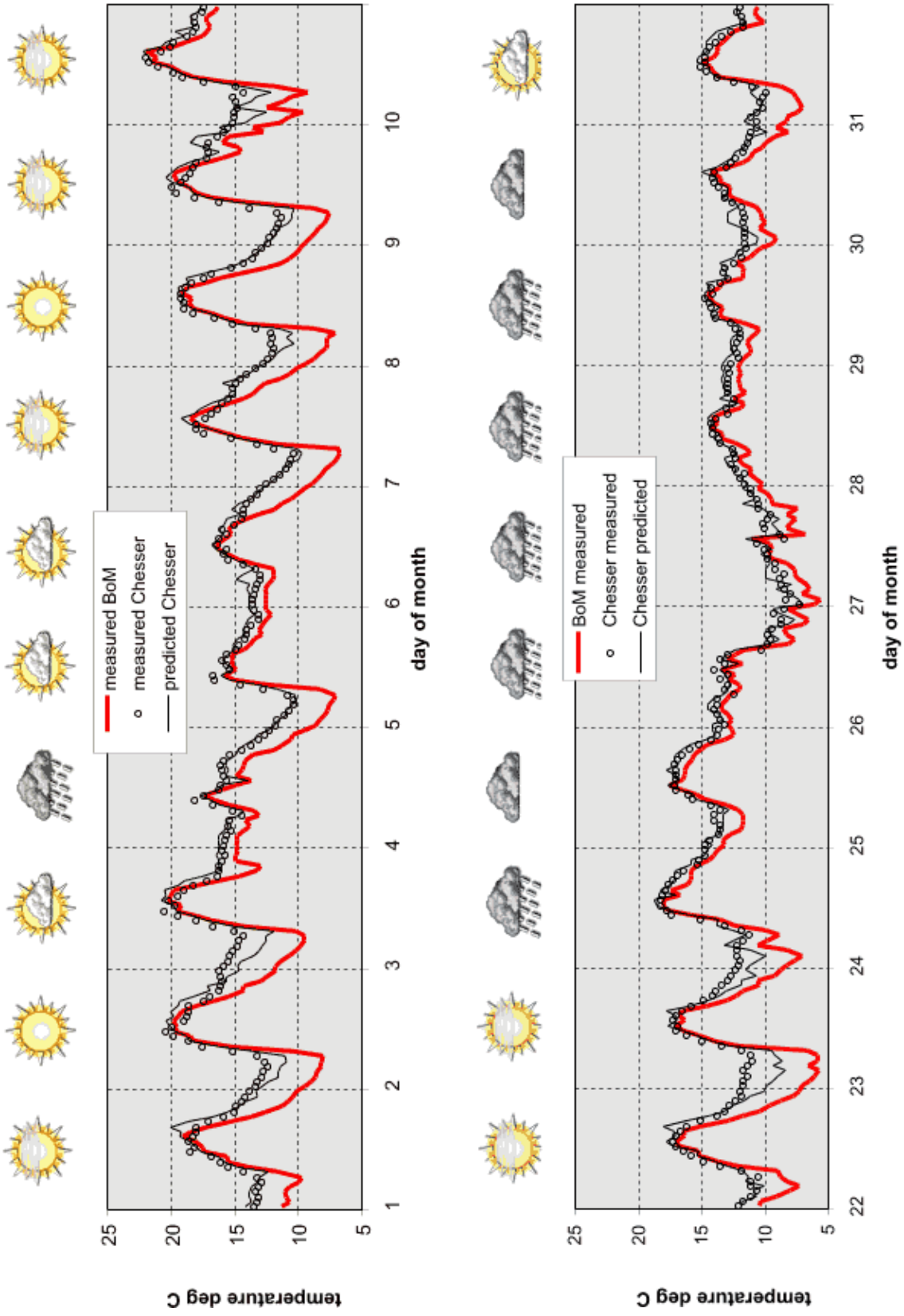

Figure 6.5: Comparison of predicted air temperature at Chesser Street with observed data for two ten-day periods in May 2000.

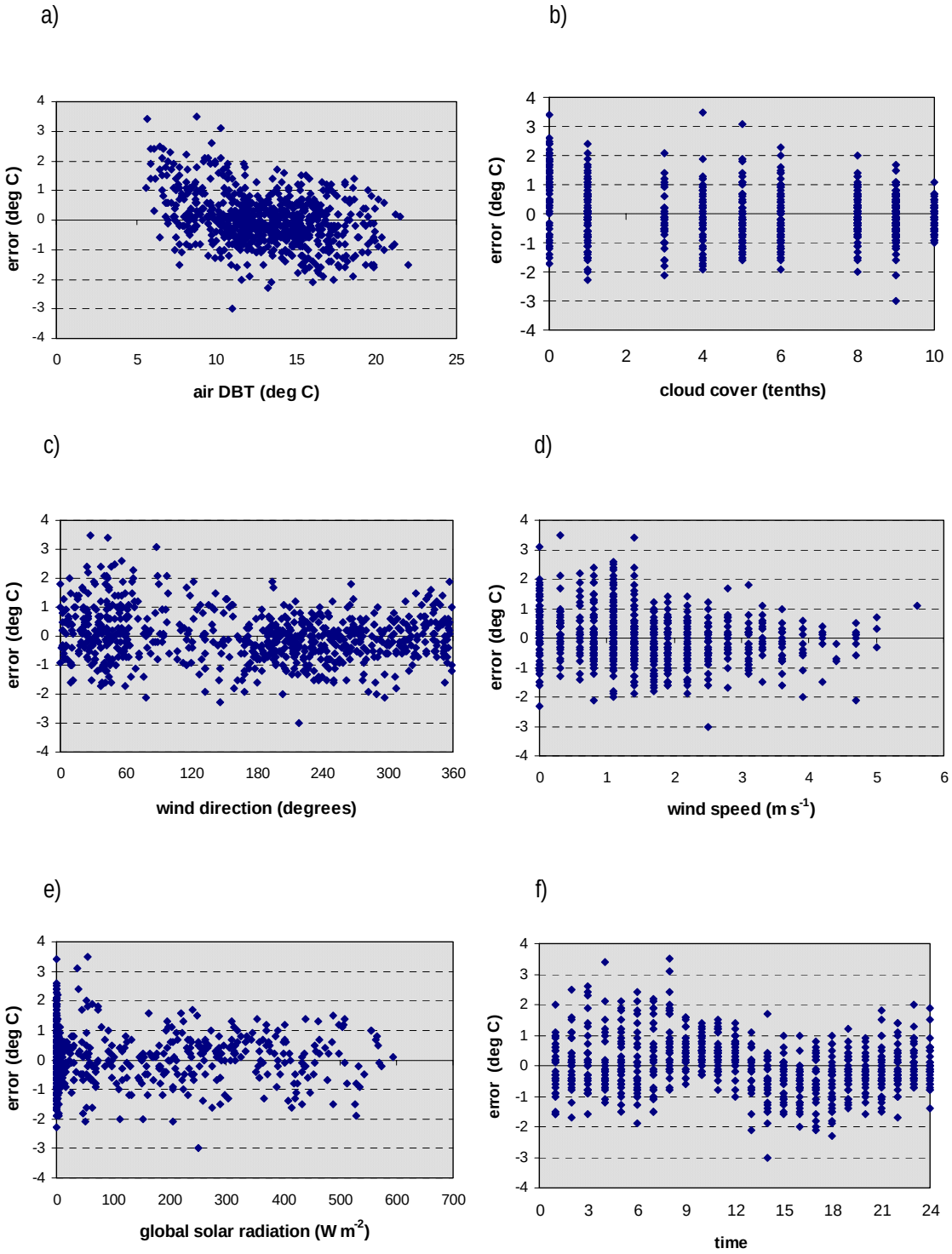

Figure 6.6: **Plot of error in predicted air temperature during May 2000 against (a) air DBT, (b) cloud cover, (c) wind direction, d) wind speed, e) global radiation and f) time of day.**

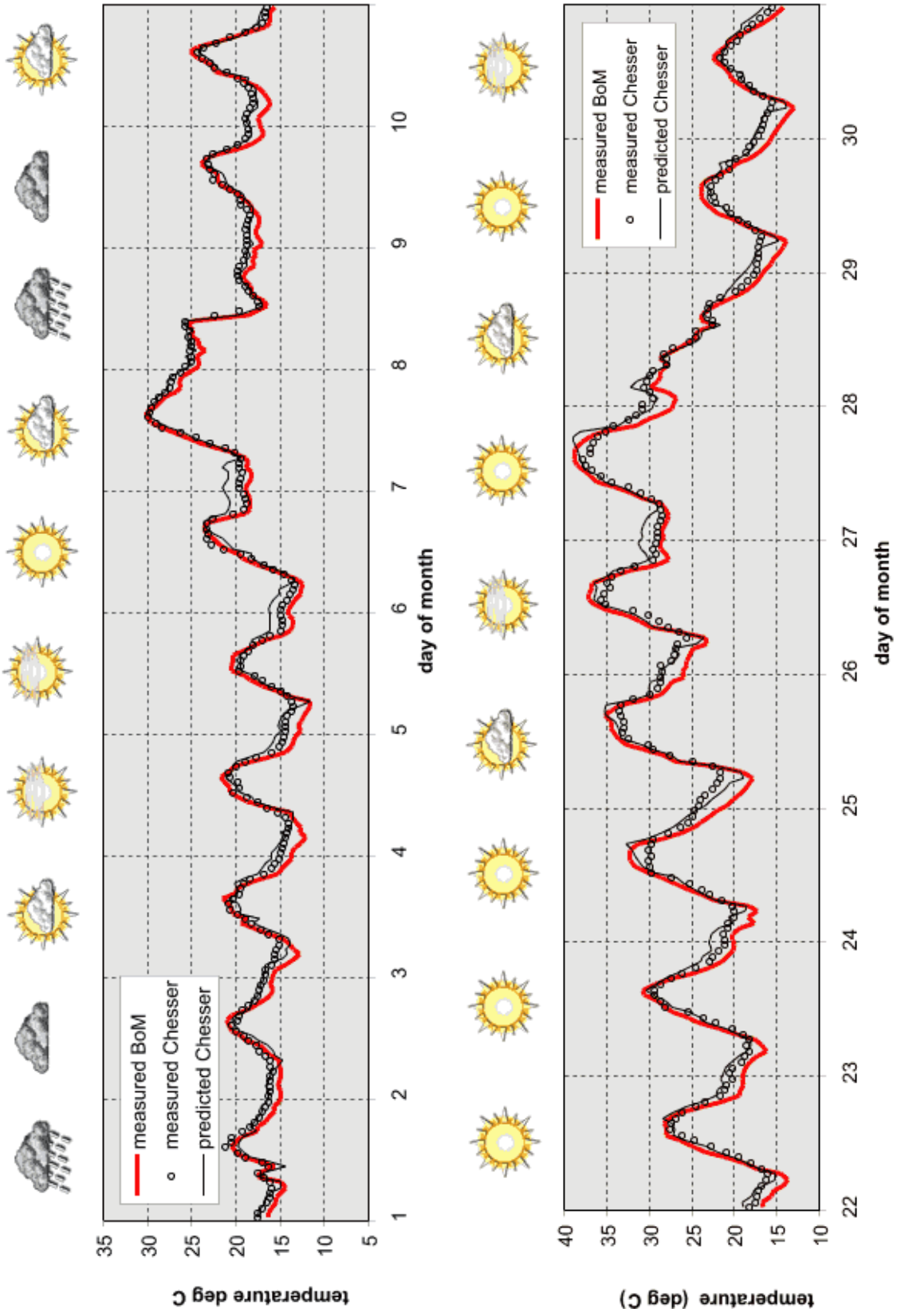

Figure 6.7: **Comparison of predicted air temperature at Chesser Street with observed data for two ten-day periods in November 2000.**

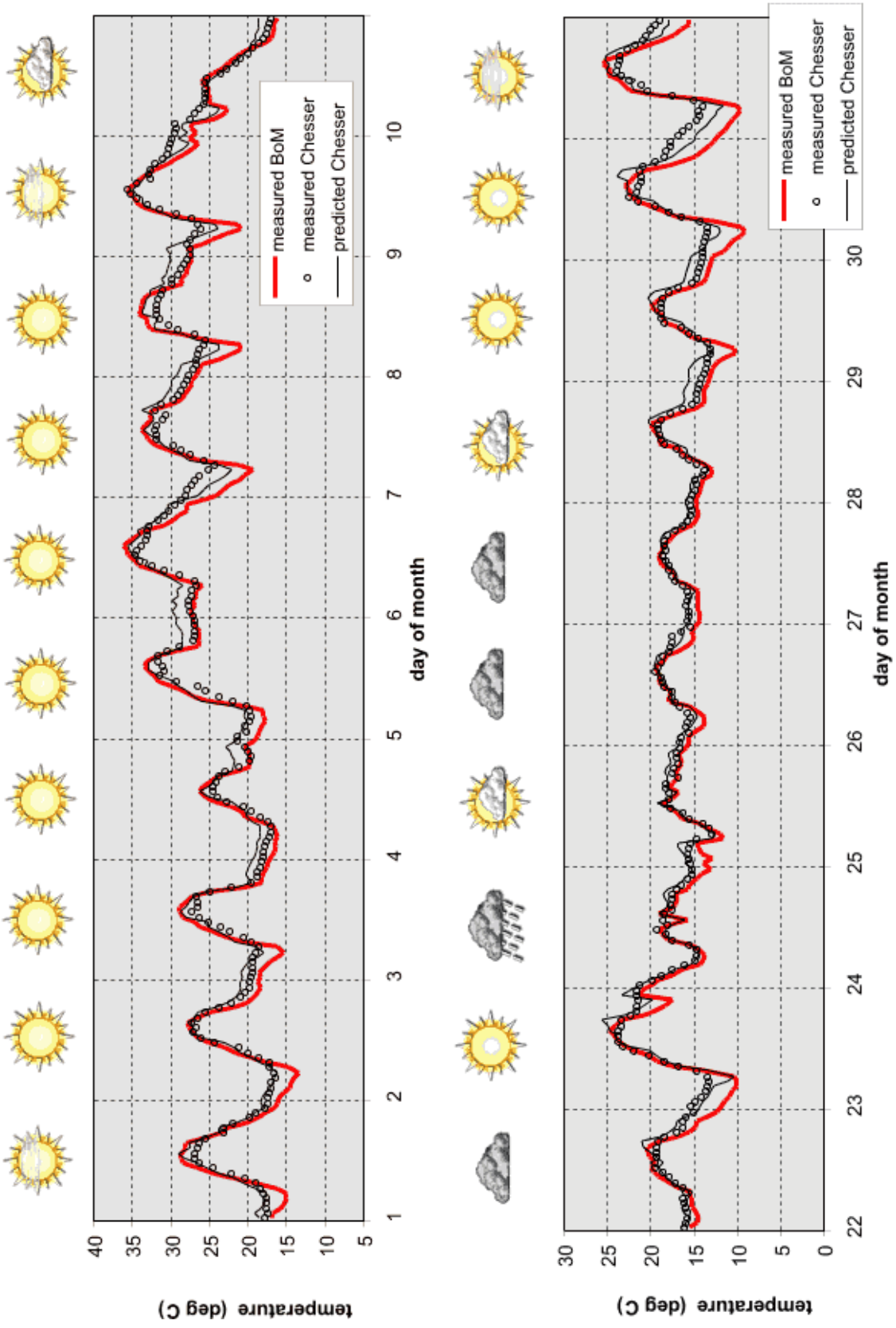

Figure 6.8: **Comparison of predicted air temperature at Chesser Street with observed data for two ten-day periods in March 2000.**

Statistical analysis

The quality of the modelled temperature prediction was assessed by comparison of the predicted and observed values of selected descriptive statistics for each month, such as the mean daily temperature (Table 6.6), and by error analysis and goodness-of-fit tests such as the Willmott index of agreement and the Williamson degree of confirmation (Table 6.7). Data were collated for four monthly periods for which complete, uninterrupted time series are available for both the BoM reference site and for the urban street canyon site. In the tables, the figures for the month of June, displayed against a shaded background, reflect the fact that the data for this month were used to calibrate the model. Figures for the other months are, however, a true test of the accuracy of CAT.

Table 6.6: Comparison of predicted and observed monthly temperature data.

	May 2000			June 2000			November 2000			March 2001		
	BoM	Chesser		BoM	Chesser		BoM	Chesser		BoM	Chesser	
		O	P		O	P		O	P		O	P
Absolute minimum	5.60	7.30	7.28	3.40	7.64	5.21	11.60	13.40	11.70	9.30	13.03	10.46
Mean minimum	9.05	10.49	10.15	11.03	12.15	11.56	20.09	21.08	20.38	14.26	15.71	14.91
Average	13.03	14.55	14.55	11.37	12.90	12.90	21.78	22.13	22.40	19.77	20.41	20.73
Mean maximum	17.13	17.29	17.79	15.35	15.51	16.22	27.24	26.34	26.94	25.25	24.43	25.37
Absolute maximum	22.00	22.00	22.28	18.80	18.84	19.46	38.90	37.80	39.01	36.30	35.74	35.61

Note: O – observed, P – predicted.

Table 6.7: Statistical evaluation of the predicted air temperature at the urban site.

	May	**June**	**Nov.**	**March**
total number of hours	744	720	720	744
mean error	0.00	0.00	-0.27	-0.37
standard deviation of the error	0.87	0.98	0.85	1.13
maximum error	3.40	4.67	2.94	4.14
minimum error	-3.14	-2.43	-3.04	-4.11
mean square error (MSE)	0.761	0.969	0.789	1.416
systematic MSE	0.016	0.163	0.103	0.18
unsystematic MSE	0.745	0.805	0.687	1.236
Wilmott index	0.974	0.956	0.993	0.988
Theil inequality coefficient	0.029	0.038	0.019	0.028
Williamson degree of confirmation	0.583	0.564	0.328	0.339

Discussion

The results of the simulation provide a number of insights:

- In all of the monthly periods simulated, the predicted air temperature in the urban canyon is a better approximation of real conditions at the site than the temperature measured at the BoM reference site.
- Both the descriptive statistics and the error analysis show that the predictions for the month of May, which was characterised by meteorological conditions similar to those in the month of June, are better than predictions for November and March, which were extremely dry.
- The comparatively lower values of the Williamson index of confirmation for the months of November and March reflect the fact that during these months the difference between conditions at the reference site and at the urban sites was much smaller than the difference during the months of May and June. Thus, although the standard deviation of the error of prediction in November is very low – only 0.85 ^{o}C – the Williamson degree of confirmation is still only about 0.33, while a similar standard deviation in May resulted in a degree of confirmation nearly twice as high – about 0.58.
- The systematic part of the mean square error is very low (in the case of May – negligible), so most of the error is unsystematic. This indicates that there are no substantial elements missing from the model, and that most of the main factors are modelled adequately.
- While the mean monthly temperature is generally predicted quite accurately, the predicted mean monthly minima and maxima both tend to be somewhat higher than observed values.
- While CAT provides predictions of mean monthly temperatures that are much closer to observed values than the default average at the BoM station, and the predicted temperature curve appears to track observed temperatures fairly closely, the code is not yet able to predict isolated incidents with the same degree of accuracy. Thus the monthly extremes of temperature (high or low) may not be predicted sufficiently accurately for the tool to be used for short periods of time. Its main utility is in providing adjustment to longer time series, such as those used to model temperature or energy consumption in the built environment over extended periods.

'Reverse' simulation

Prediction of air temperature using the CAT model is carried out in two steps: First, the base temperature is derived by subtracting from the measured air temperature at the reference station a temperature modification resulting from the microclimatic effects of the site; the microclimatic modifications resulting from the site-specific conditions at the urban site are then added to the base temperature, thus obtaining the predicted air temperature. The CAT model does not pose any special requirements with respect to the characteristics of the reference site or the urban site, except for limitations resulting from the capacity of the wind model to

predict wind speed near each of the canyon surfaces. The code may therefore be used to model air temperature in an urban street canyon on the basis of reference data at a standard meteorological station – but it should also be able to perform the reverse simulation, and predict air temperature at an exposed site on the basis of urban air temperature. Furthermore, since the base temperature is always calculated as an interim step in the simulation process, and since it is assumed to be spatially homogeneous (within the limits of the relevant area), its value should be the same irrespective of the location and physical properties of the reference site.

These assumptions were tested using data for the month of May 2000. The simulation was carried out twice: First, the air temperature at the Chesser Street urban site was predicted on the basis of measured data from the reference site at the BoM station at Kent Town (the 'forward' simulation). Then measured data from the Chesser Street site were used to predict temperature at the Kent Town BoM station (the 'reverse' simulation). The base temperature was therefore calculated independently twice, providing a direct test of the assumptions regarding independence of location and spatial homogeneity.

Figure 6.9(a) shows two time-series representing the interim 'base temperature' for a sample period of ten days. The lines are clearly similar; a test of linear correlation on the basis of data for the entire month gave a line of best fit with a slope close to unity and a very small offset ($y = 0.87x + 1.44$), and $r^2=0.91$. The close correlation indicates that there are no major unexplained factors missing from the model. Furthermore, since both calculations of the base temperature are based on real site data, measurement errors are responsible for at least part of the variance.

Further support for the underlying concept of the model, which relates screen level temperatures and surface modifications to a spatially homogenous mixed layer above the buildings of the city, is found in the complete results of the 'reverse' simulation, in which air temperature at the BoM station was predicted on the basis of urban air temperature (Figure 6.9 (b) and Table 6.8). The impression given by visual inspection of the graph is supported by the error statistics, namely that the reverse simulation is as accurate as the forward one.

Table 6.8: Statistics of 'reverse' simulation for prediction of air temperature at BoM site from measured urban air temperature.

	May
total number of hours	744
mean error	0.00
standard deviation of the error	0.87
maximum error	3.40
minimum error	-3.14
mean square error (MSE)	0.761
systematic MSE	0.128
unsystematic MSE	0.633
Wilmott index	0.981
Theil inequality coefficient	0.032
Williamson degree of confirmation	0.54

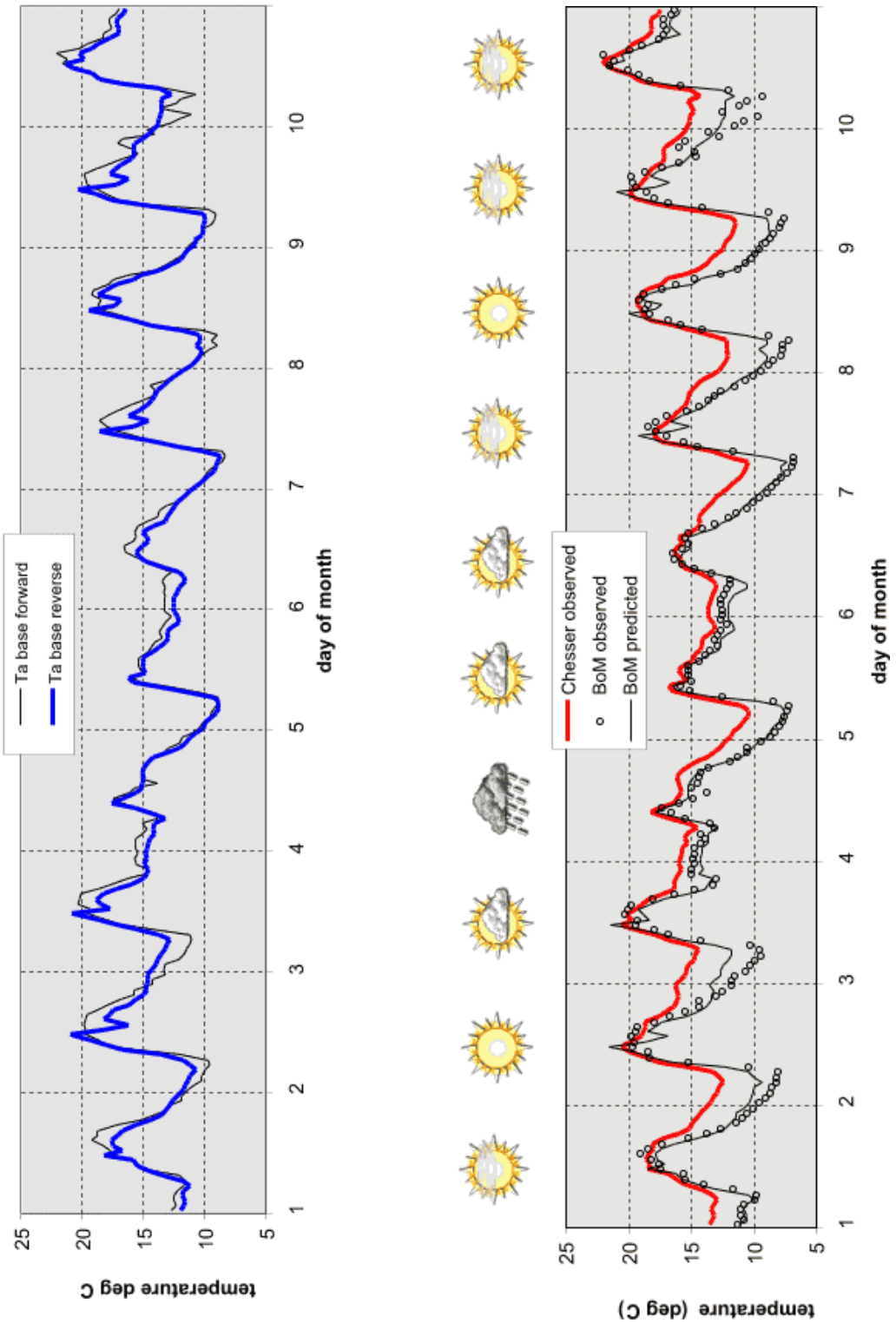

(a) (b)

Figure 6.9: **Sample results of the 'reverse simulation' for the first 10 days of May 2000: a) Base temperature calculated by means of the 'forward' and 'reverse' simulations, and b) Air temperature at the BoM reference site predicted from measured air temperature at Chesser Street.**

Effect of orientation

Simulation studies with CAT indicated that the orientation of relatively deep street canyons has an effect on the diurnal evolution of air temperature. This effect is due to differences in penetration of direct solar radiation into the canyon: East-west canyons are exposed to direct solar radiation early in the morning and late in the afternoon, while canyons with a north-south axis allow the sun to penetrate near mid-day. On sunny days and in the absence of vigorous mixing by wind one may therefore expect north-south canyons to be warmer than east-west ones near the middle of the day (Figure 6.10). Because the intensity of radiation is lower in the morning and in the afternoon, the reverse effect is, however, much weaker.

Experimental data bear out this finding. Figure 6.11 shows the corresponding measured difference in air temperature between Chesser Street (north-south axis) and the adjacent French Street (east-west axis), plotted against time of day (based on May 2000 data). Even allowing for a much larger variance in the measured data, the difference between the two streets is easily apparent.

The calculated correlation between measured and predicted temperature difference between the two streets is modest: R^2=0.22. However, the trend is nevertheless present, as the CAT model suggests. The larger magnitude of the difference in the measured data may be explained in part by imperfect screening of the temperature sensors, in spite of the effort made to protect them (Chapter 4), although the maximum error arising from this factor is estimated at no more than 1 ^{o}C. If this explanation is correct, then the air temperature in Chesser Street near mid-day, when the instrument screens were exposed to direct sunlight, may in fact be somewhat lower than recorded values and the difference between the two streets – though still substantial - correspondingly smaller.

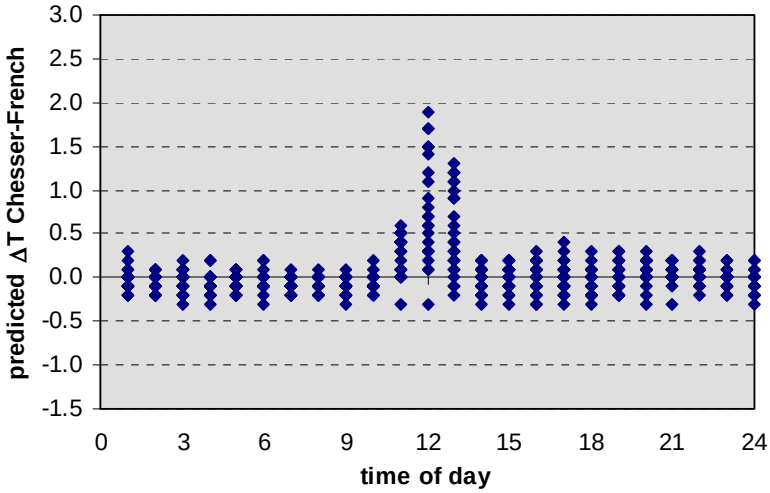

Figure 6.10: Predicted difference in air temperature between Chesser Street (north-south axis) and French Street (east-west axis) based on May 2000 data. Positive values indicate Chesser Street is warmer.

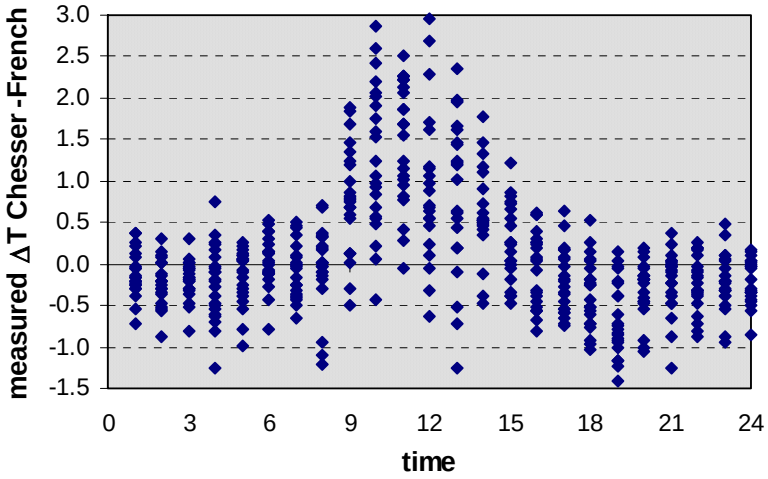

Figure 6.11: **Measured difference in air temperature between Chesser Street (north-south axis) and French Street (east-west axis), ensemble data for May 2000. Positive values indicate Chesser Street is warmer.**

CHAPTER 7: APPLICATION, DISCUSSION AND CONCLUSIONS

7.1 Introduction

Research on urban climatology has made great progress in the past three decades, and most of the main mechanisms involved in the development of unique microclimatic conditions in urban street canyons are well understood. However, as the review in Chapter 2 shows, integrated predictive models designed for urban planners are not yet available, so practical application of this understanding in the design of buildings and cities is still very limited. Subsequent chapters have described a modelling framework aimed at providing a tool that responds to this shortcoming: Chapter 3 established the theoretical basis of the scheme; Chapter 4 described an experimental monitoring program to obtain field data required to calibrate and validate the model; Chapter 5 presented the main findings of this experiment, which were then applied in Chapter 6 to establish the validity of the CAT model, at least under certain environmental conditions.

The present chapter will attempt to evaluate the benefits of applying the CAT model to modify reference climate data to account for urban modifications, and to assess the limitations of the model in its current state of development. It concludes with a proposed program of further development recommended to improve the utility of CAT and to overcome restrictions on its application.

7.2 Application of the CAT computer model

The CAT model may be used to generate realistic, site-specific temperature inputs for building thermal simulation software, required to produce more accurate modelling of energy use. It may also be used to evaluate the effect on micro-climatic conditions of proposed development at new urban locations.

The model has two types of inputs: meteorological data from a reference site, and a description of both the reference site and the urban site in the form of various parameters. Modification of the input describing a theoretical urban site will allow a study of the effects of each of the parameters on the air temperature at the simulated location.

Description of the two sites requires the following inputs by the user:

- Values of parameters describing site morphology, such as the canyon width and height.
- Values of parameters describing properties of materials comprising the sites, including albedo, moisture availability and heat storage coefficients for the ground and walls.

Planners may influence many of the above factors during the preparation of urban master plans or neighbourhood layouts, thus affecting the temperature in the urban canopy layer. A parametric study based on the computer model may be used to quantify the scale of temperature modification it may be possible to achieve in a city with a climate similar to that of Adelaide. Such a study illustrates a potential application of an urban climate model of the type proposed in this research project. Similar parametric studies involving the input of meteorological data from other climatic zones may be used to highlight different planning strategies suitable for different environments, such as the tropics or deserts.

7.3 Practical example

To demonstrate the effect of taking into account urban modifications of air temperature, a simple simulation of the performance of a building was carried out using the EnerWin whole-building energy simulation software ((Degelman and Soebarto, 1995; Soebarto and Degelman, 1995). The simulation was performed twice. First the energy performance was carried out using Adelaide meteorological data from the Australian Climate Data Bank to describe environmental conditions. The same building was then simulated a second time, using a modified input file with air temperature in a hypothetical urban canyon predicted by CAT in place of measured air temperature data from BoM Kent Town. The results of the simulations were then compared to assess the effect of urban modifications to air temperature on the energy budget of the building.

Modifications to climate input file

EnerWin requires input of environmental data in the form of hourly records for an entire year. For this study, weather data in TMY2 format were used. Data recorded at the Kent Town BoM weather station in 1987 were formatted accordingly and used to simulate the base case.

The same data were then processed to conform to the input format of CAT, and the software was run to produce a time series of predicted air temperature in an urban canyon. The site parameters used by CAT to describe the Chesser Street urban canyon were also used in the present simulation to describe the hypothetical urban site. No account was taken of differences between air temperatures in streets of different orientations, however. A single value corresponding to the air temperature in a north-south canyon was used as a representative input: EnerWin, like most whole-building simulation software, assumes all external building surfaces are exposed to a uniform ambient air temperature.

Figure 7.1 shows the difference in air temperature between the simulated urban environment and the measured Kent Town data for each hour for the entire year, plotted against time of day. The comparison is instructive: The urban site is warmer than the reference site by 0.5-3.2 ^{o}C throughout the night, but urban temperatures during the daytime are often cooler - the temperature difference $\Delta T_{u\text{-}r}$ at noon ranges from about 1.1 ^{o}C to about -2.2 ^{o}C.

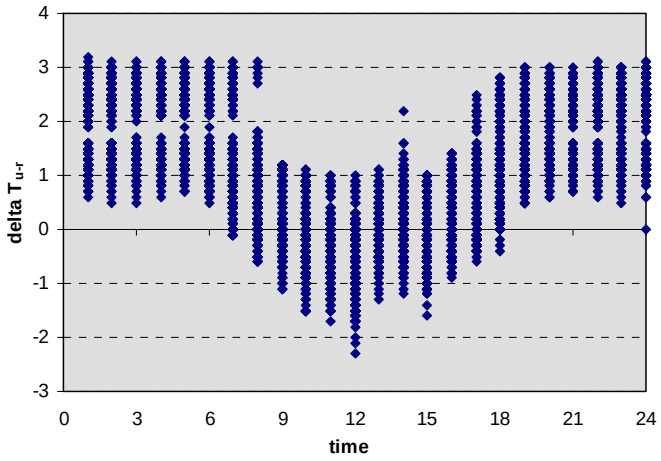

Figure 7.1: Diurnal pattern of the Adelaide urban heat island, simulated for an entire year using CAT. (Input data are for 1987).

Figure 7.2 shows that in addition to distinct diurnal pattern, there is a clear annual pattern to the temperature difference. During winter (May-August), the urban heat island is an almost continuous feature, both day and night, varying only in magnitude. During the rest of the year, and especially during the summer months, the nocturnal urban heat island alternates with a weak daytime cool island. These effects were also seen in the measured data collected as part of the research: The mean daily temperature in the Chesser Street site was 1.53 ^{o}C higher than the temperature in the Kent Town BoM site during the winter month of June and 1.52 ^{o}C higher in May - but only 0.35 ^{o}C higher in November and 0.64 ^{o}C higher in March (See Table 6.6 above).

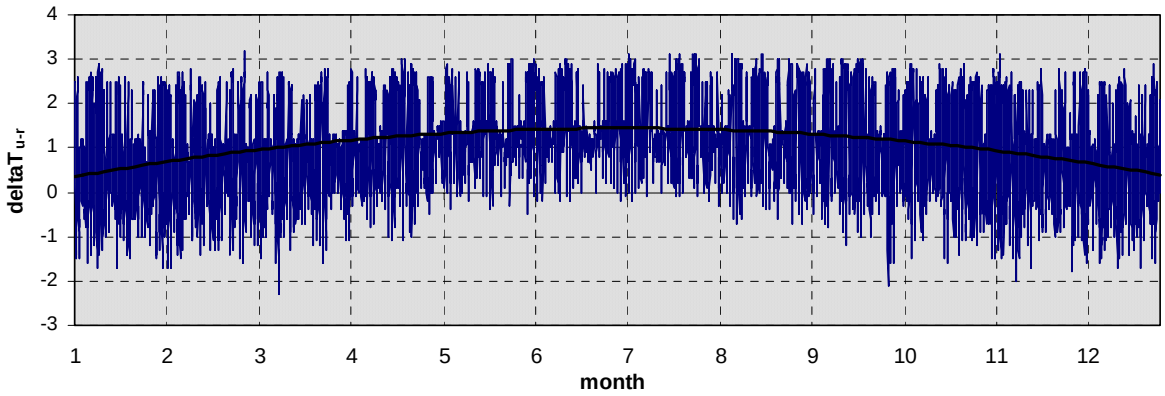

Figure 7.2: Seasonal pattern of the urban heat island of Adelaide simulated by CAT on the basis of meteorological data for 1987.

Building description

The building selected for the simulation study is the sample building included in the EnerWin software (except that the number of floors was reduced to four). It is a multi-use building with four almost identical rectangular floors which have their long axis oriented east-west. Each floor comprises offices, laboratories and classrooms arranged around a central corridor so that each has at least one exterior wall (See Figure 7.3.). The total floor area of the building is 6536 m^2 (about 60m x 30m per floor).

The simulated building has external walls of insulated masonry blocks (thermal conductance U=0.79 W m^{-2} K^{-1}), a built-up roof (U=0.33 W m^{-2} K^{-1}) and concrete slab intermediate floors. An infiltration rate of 0.4 air changes per hour was specified, and in addition a (mechanical) ventilation rate of 0.7 l s^{-1} m^{-2}. Internals heat gains are calculated taking into account a detailed occupancy schedule, whereby the building is occupied 5 days a week, with a varying number of occupants for each hour. Lighting and equipment introduce an additional load of 18 W m^{-2}, on average.

The simulated HVAC system incorporates a central air conditioning plant with a COP of 2.64 in the cooling mode, and heating by gas, with an assumed COP of 0.7. Thermostat settings for the simulation were: summer: 24 ^{o}C (when the building is occupied) and 26 ^{o}C (when it is unoccupied); and winter: 22 ^{o}C (occupied) and 20 ^{o}C (unoccupied).

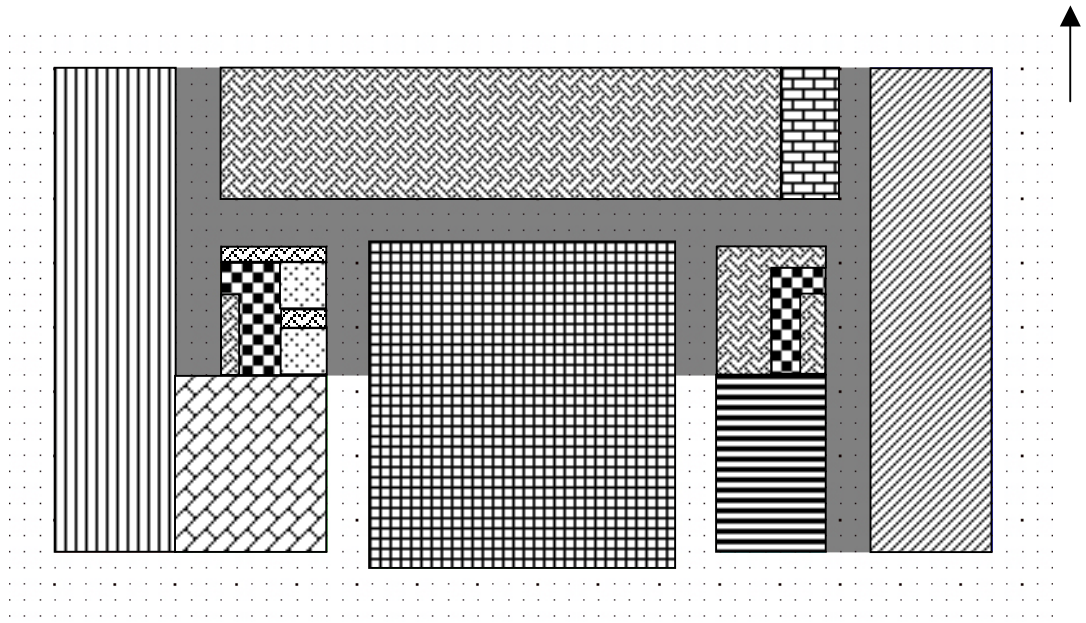

Figure 7.3: Floor plan of the building used in the EnerWin simulation. (Image adapted from the EnerWin input screen. Hatch patterns represent different functional zones, e.g. office, classroom, laboratory, corridor, toilets.)

Simulation results

EnerWin calculates hourly energy transfer through each of the building elements, in addition to loads resulting from occupants and equipment, and the total load on the HVAC system required to maintain the specified set point temperature, in either heating or cooling. In addition to peak loads, which must be predicted by the engineer in order to size system components, EnerWin calculates the total energy consumption on an annual basis, allowing the user to predict the economic cost of providing thermal comfort.

Table 7.1 shows the peak loads through each of the building components for the base case (part A) and for the CAT modified input (part B). The values at the bottom of each part of the table indicate the peak load on the HVAC system for heating and for cooling. Comparison of the results shows that when these values are calculated using the input modified for urban conditions, there is a reduction of 6.0% for heating, from 344.8 kW to 325.2 kW, and a reduction of 2.95% in peak cooling, from 402.7 kW to 391.2 kW.

Similarly, Table 7.2 shows the annual heat gain or loss through each of the building components for the two simulations, and the total annual energy consumption for heating or cooling. Comparison of the results shows that the predicted energy consumption for heating was 25.8% lower when the calculation was carried out using the modified data: 842.2 GJ compared with 1059.7 GJ in the base case. Predicted cooling loads were, on the other hand, 14.7% higher: 670.9 GJ compared with 572.2 GJ in the base case. The total annual energy consumption predicted using the modified data was 1513.1 GJ, or about 7.3% less than the prediction based on raw climate data, which was 1631.9 GJ.

The reduction in peak loads for both heating and cooling is not surprising, since the urban fabric has the effect of damping extreme diurnal variations in temperature, reflected both in the nocturnal heat island and in the (smaller) daytime cool island. Likewise, the reduction in the annual heating budget and increase in cooling reflects the fact that the city is, on average, warmer than the base station for most of the year.

While the trends illustrated by the simulation with respect to the heating and cooling requirements can be explained in a qualitative manner, it is the quantitative nature of the results that is important. The ability to predict accurately both peak loads on HVAC equipment and total annual heat consumption is of great value in the design of HVAC systems and in economic calculations regarding their operation and maintenance. The design of such systems is routinely carried out using detailed whole-building energy simulation models. As this example illustrates, failing to account for urban modifications to air temperature may lead to errors that are too large to overlook. HVAC plant may be either over–sized or too small, leading to unnecessary expenditure in the first instance or to failure to cope adequately with loads in the latter. Any optimisation of life cycle costs of the equipment can only be done if the capital cost is realistic and if running costs are estimated accurately. Finally, certification of the performance of the building within the framework of a building energy-rating scheme, a procedure that is now required by an increasing number of local authorities in many countries, might be affected if local climate modifications are not accounted for. This has legal and financial implications that should not be ignored.

Table 7.1: Effect of applying CAT to climate input data for EnerWin simulation of peak power requirements of typical office building in Adelaide.

a) Base case: original Bureau of Meteorology data

load categories	peak gain/loss (kW)			
	heating	% total	cooling	% total
roof	-6.9	-2.0	3.7	0.9
walls	-45.5	-13.2	19.0	4.6
windows transmission	-25.2	-7.3	16.5	3.9
windows solar	20.5	5.6	38.8	9.3
lights and equipment	0.0	0.0	148.7	35.7
people and sensible	31.2	8.3	30.9	7.4
people latent	0.0	0.0	24.7	5.9
infiltration/ventilation	-113.6	-33.0	134.3	32.2
mass effect	-153.6	-44.6	-13.8	-3.3
central plant peak load	**-344.8 kW**		**402.7 kW**	

b) Bureau of Meteorology data modified by CAT to account for urban conditions

load categories	peak gain/loss (kW)			
	heating	% total	cooling	% total
roof	-6.0	-1.9	5.1	1.3
walls	-39.5	-12.1	25.3	6.5
windows transmission	-23.4	-7.2	22.8	5.8
windows solar	20.5	5.9	14.5	3.7
lights and equipment	0.0	0.0	150.4	38.3
people and sensible	31.2	8.7	31.2	7.9
people latent	0.0	0.0	25.0	6.4
infiltration/ventilation	-105.0	-32.3	118.2	30.1
mass effect	-151.3	-46.5	-1.3	-0.3
central plant peak load	**-325.2 kW**		**391.2 kW**	

Note: Ener-Win allows input of internal loads to simulate the effect of lights and equipment. However, these loads are not taken into account when the peak heating load is calculated, to ensure that the heating system can handle the entire load in case this equipment is not actually turned on at the time. This explains the 'zero' value for this category in the tables above. The load generated by lights and equipment is, however, accounted for both in the cumulative calculations carried out to assess the annual energy requirements and in the calculation of the peak load on the cooling system.

Table 7.2: Effect of applying CAT to climate input data for EnerWin simulation of annual energy consumption of typical office building in Adelaide.

a) Base case: original Bureau of Meteorology data

load categories	annual gain/loss (GJ)			
	heating	% total	cooling	% total
roof	-37.9	-1.8	11.1	1.6
walls	-372.8	-18.1	11.7	1.7
windows transmission	-112.4	-5.5	15.6	2.3
windows solar	111.9	9.6	39.9	5.9
lights and equipment	777.2	42.3	363.7	53.7
people and sensible	109.8	9.4	100.0	14.8
people latent	0.0	0.0	80.0	11.8
infiltration/ventilation	-1296.6	-63.0	54.8	8.1
mass effect	-238.9	-11.6	-104.7	-15.5
total annual loads	**-1059.7 GJ**		**572.2 GJ**	

b) Bureau of Meteorology data modified by CAT to account for urban conditions

load categories	annual gain/loss (GJ)			
	heating	% total	cooling	% total
roof	-28.5	-1.6	12.4	1.6
walls	-299.6	-16.9	14.4	1.9
windows transmission	-103.2	-5.8	14.7	2.0
windows solar	108.7	11.4	46.7	6.2
lights and equipment	727.0	46.3	414.6	55.0
people and sensible	98.3	10.5	111.7	14.8
people latent	0.0	0.0	89.4	11.8
infiltration/ventilation	-1056.9	-59.5	50.5	6.7
mass effect	-288.0	-16.2	-83.5	-11.1
total annual loads	**-842.2 GJ**		**670.9 GJ**	

7.4 Advantages, restrictions and limitations of CAT

The CAT model is predicated on the proposition that the properties of the roughness sublayer immediately above the canopy layer are, on the average, uniform over an area in which both the reference station and the urban canyon are located. Where this condition cannot be met – and extensive research has shown that in large urban centres with extremely dense cores anthropogenic heat flux can result in urban heat islands in the mixed layer – the CAT model must be coupled to a meso-scaled model capable of simulating these differences. Since CAT calculates the total sensible heat flux generated in a canyon, there should be no difficulty in doing so, although this has not been attempted in practice. The CAT model is also incapable of analysing differences between the reference site and the urban canyon resulting from meso-scale properties of the sites such as topography, elevation, distance from the a large body of water (if applicable) etc.

The CAT model, in common with many models of the urban microclimate, assumes that net advective heat transfer within the urban area is negligible. It is clearly applicable where building density, typology and ground cover in the source area for energy fluxes are approximately homogeneous. However, measurements made in the urban sites as part of this research suggest that the presence of urban parks or large variations in building height and street sections in the source area of the airflow advected to them may have only a minor effect on canyon air temperature. There is need for further field research to establish the magnitude of the effect on canyon air temperature of such meso-scale features, taking into account their distance from the street in question, the direction of the wind and the intensity of the fluxes.

Calculation of net radiant flux at the surface (Q*) incorporates the sol-air temperature as an approximation of the real surface temperature. This has been shown to result in negligible errors in the case of exposed soil surfaces, but might result in larger errors if the methodology is applied to other types of surfaces:

- Vegetated surfaces, whose temperature is regulated by evapotranspiration and sometimes by radiant and convective exchange with sub-canopy surfaces.
- Thin materials not coupled to a substantial thermal mass, which may experience very large and rapid changes in temperature in response to changes in radiant flux.

The CAT model uses empirical correlations to estimate the convective heat transfer coefficient h_c from wind speed near the surface (Equations 3.10 and 3.11). This value of this coefficient is then incorporated in the calculation of the sol-air temperature of each of the canyon surfaces and in the overall heat transfer from the canyon system to the roughness sublayer. It would therefore appear that accurate determination of the coefficient has a direct bearing on the quality of the model predictions. However, the nature of the correlations, which are in the form of a sum of a constant factor and a wind-related one, is such that the value of h_c is relatively insensitive to changes in the wind at low speeds, and more so at high speeds. The magnitude of the absolute error in prediction resulting from an inaccurate estimate of the convective heat transfer coefficient is therefore in practice fairly small: In windy weather air temperature in the urban street canyon is likely to be very similar to the temperature of the surroundings, as reflected in the high value of the

mixing ratio *m* for turbulent conditions. In relatively calm weather, the absolute error in the estimate of h_c is likely to be small, resulting in a proportionately small error in the prediction of canyon air temperature. Nevertheless, improving the accuracy of the estimate for h_c in urban configurations where canyon air flow is not characterised by a simple rotor vortex – either because the canyon is too shallow (resulting in isolated roughness flow, according to Oke's classification) or because it is very deep (resulting in very weak coupling of street-level wind with air above the canyon) – remains a priority for future development of the model.

Assessment of the sensible heat flux is sensitive to the value of the coefficient α in equations 3.15 and 3.16 above. This coefficient, which describes the availability of moisture in different environments, may range in value between zero in hyper-arid locations to about 1.4 over oceans (Grimmond and Oke, 2002). In most urban sites it is likely to be in the range 0.2-1.0, but a more accurate determination may require calibration of the CAT model to a variety of locations on the basis of experimental data from on-site monitoring. Until such data are available, calibration may be carried out to fit predictions to data from the reference site in meteorological conditions that are known to result in negligible urban effects, such as windy, overcast weather. This procedure may only be carried out if the contribution of anthropogenic heat to temperature differences between the locations is small.

CAT uses an empirical correlation between the sol-air temperature of an exposed reference surface and a coefficient of mixing between the urban canopy and the mixed layer above roof height. Accuracy of model predictions is sensitive to values of this coefficient, so further examination of this procedure and validation against observed data in a variety of environmental conditions are required before the model can be applied with confidence in climates or urban morphologies that are very different from Adelaide.

7.5 Conclusion

Work reported upon in the previous chapters confirms the research hypothesis, namely "that a relatively simple uncoupled model of the temperature in the urban canopy, i.e. a model in which there is no feedback from the micro-scale site to the meso-scale urban boundary layer, can predict the temperature at a given site with sufficient accuracy to be a useful tool for simulation of the effects of urban form on site-specific air temperature".

The aim of this project was to create a model capable of simulating weather conditions for extended periods, with simplified inputs and less detailed, yet accurate, outputs. The CAT (Canyon Air Temperature) computer model predicts site-specific air temperature in a city street based on data from a rural reference station. In addition to a rudimentary description of the two sites, it requires only inputs measured at standard weather stations, yet is capable of predicting accurately the evolution of air temperature in all weather conditions for extended periods. It simulates the effects of urban geometry on radiant exchange; the effect of moisture availability on latent heat flux; energy stored in the ground and in building surfaces; air flow in the street based on wind above roof height; and the sensible heat flux from individual surfaces and from the street canyon as a whole.

The model was validated using field data recorded over a period of almost a year in several locations in Adelaide. Comparison of observed and predicted air temperature using standard descriptive statistics such as means, maxima and minima, as well as more advanced analysis of errors in prediction using techniques such as the Williamson confirmation factor, demonstrates that once calibrated for specific local conditions the CAT model is capable of providing time series of air temperature in an urban street canyon that are significantly closer to real temperature than measurements made at a standard meteorological station in the metropolitan area.

Application of the model to provide modified meteorological input data to a whole-building energy simulation model demonstrated the importance of the tool if accurate results are to be expected.

7.6 Future research

The utility of any computer simulation program depends, *inter alia*, on the confidence potential users have in the quality of the predictions. Testing the code on other meteorological databases in diverse geographic locations may thus contribute to its acceptance. This may appear like a trivial conclusion, but its application in practice may not be straightforward: There are very few accurate, well-documented records of environmental conditions in city-centre locations and in adjacent reference stations for sufficiently long periods of time to enable calibration of the code to simulate conditions different to those found in Adelaide.

CAT has been shown to perform well in a variety of weather conditions, but is restricted to simulating relatively deep urban canyons in which a rotor flow is likely to be generated in most weather conditions. This type of street is one in which conditions are most likely to be substantially different from a rural reference site, but extending the wind model to other urban geometries may nevertheless be a valuable addition to the tool.

The calculation of sensible heat flux requires parallel modelling of latent heat flux. This information may be used in turn as the basis for a model of urban modification of atmospheric humidity. A model capable of predicting humidity in the vicinity of urban buildings would provide more accurate input of climatic data to whole-building thermal simulation programs, especially those that calculate the performance of air conditioning systems, which are affected not only by the temperature of ambient surroundings but by atmospheric humidity. Such a model could also drive calculations of human thermal comfort in outdoor urban spaces such as streets and plazas, and assist in the planning of more pedestrian-friendly environments.

Finally, CAT – or Canyon Air Temperature, was developed to model conditions in an urban street canyon. This morphological unit has been used almost exclusively in studies of the urban microclimate, for a variety of reasons. However, many urban spaces cannot be modelled by a hypothetical, semi-infinite two-dimensional channel with walls of uniform height. Modelling the full complexity of urban space may require a much more complex framework than CAT – but the benefits of applying some of the insights gained in developing the model are proportionately greater.